



Distinct medial amygdala oxytocin receptor neurons projections respectively control consolation or aggression in male mandarin voles

Received: 10 February 2023

Accepted: 12 August 2024

Published online: 17 September 2024

 Check for updates

Yishan Qu ^{1,2}, Lizi Zhang^{1,2}, Wenjuan Hou¹, Limin Liu¹, Jing Liu¹, Lu Li¹, Xing Guo¹, Yin Li¹, Caihong Huang¹, Zhixiong He¹  & Fadao Tai ¹ 

The individuals often show consolation to distressed companions or show aggression to the intruders. The circuit mechanisms underlying switching between consolation and aggression remain unclear. In the present study, using male mandarin voles, we identified that two distinct subtypes of oxytocin receptor (OXTR) neurons in the medial amygdala (MeA) projecting to the anterior insula (AI) and ventrolateral aspect of ventromedial hypothalamus (VMHvl) respond differently to stressed siblings or unfamiliar intruders using c-Fos or calcium recording. Oxytocin release and activities of PVN neurons projecting to MeA increased upon consoling and attacking. OXTR antagonist injection to the MeA reduced consoling and attacking. Apoptosis, optogenetic or pharmacogenetic manipulation of these two populations of neurons altered behavioral responses to these two social stimuli respectively. Here, we show that two subtypes of OXTR neurons in the MeA projecting to the AI or VMHvl causally control consolation or aggression that may underlie switch between consolation and aggression.

Consolation and aggression are cross-species conserved and representative types of pro-social and anti-social behaviors, respectively, in animals. Whether individuals show consolation or aggression depends on whom they encounter displaying behavioral flexibility. The flexibility that individuals display optimal behavioral responses in different social contexts is crucial for individual well-being, survival, and stability of mammal species^{1,2}. In addition, the comorbid abnormalities in prosociality and aggression are associated with multiple mental disorders, such as less prosociality in autism (ASD)³ and schizophrenia⁴, and more aggression in bipolar (BD) and major depression disorder (MDD)⁵. However, the neural circuits underlying switching between the consolation and aggression remain unclear.

It is well-known that endogenous oxytocin (OXT) regulates consolation^{6–8} and aggression^{9–11}. OXT receptors (OXTR) are

abundantly distributed in the medial amygdala (MeA)^{12,13}, which is a key brain node to generate corresponding social decision-making by identifying and processing various odor information in different social contexts¹⁴. OXT signaling is involved in the generation of long-term social recognition by altering MeA synaptic plasticity^{15,16}. Injection of the mRNA gene's antisense oligonucleotides or antagonists of OXTR into the MeA impaired social cognition and reduced social approach behaviors^{17,18}. Given the fact that OXTR in the MeA regulates social motivation, which may be the basis of prosocial behaviors¹⁹, it may affect consolation². The MeA also regulates aggression in a precise and extensive manner through different projections to the ventrolateral region of the ventromedial hypothalamus (VMHvl) and bed nucleus of the stria terminalis (BNST)²⁰. One study has revealed a negative correlation between levels of aggression and MeA OXT mRNA during

¹Institute of Brain and Behavioural Sciences, College of Life Sciences, Shaanxi Normal University, Xi'an, Shaanxi, China. ²These authors contributed equally: Yishan Qu, Lizi Zhang.  e-mail: hezixiong@snnu.edu.cn; taifadao@snnu.edu.cn

lactation⁹. Whether and how the OXT signaling in the MeA affected aggression remains unknown. Thus, we hypothesized that the OXT via binding with OXTR in the MeA may control consolation and aggression in different social contexts as an underlying mechanism of behavioral flexibility.

The MeA receives olfactory cues from intruders and distressed partners, and then controls the occurrence and development of attack and allogrooming through projections to different targets such as MeA–VMHvl/BNST and MeA–Medial preoptic area (MPOA) pathways that control aggression²⁰ and consolation²¹, respectively. The anterior insula (AI) converges sensory (including olfactory) input and connects regions implicated in emotion processing like the amygdala, and consequently controls empathetic behaviors possibly^{22–24}. Its involvement in empathetic behaviors has been demonstrated in humans by neuroimaging²⁵ and in rodents by invasive mechanistic research²⁶. Correspondingly, the VMHvl that also receives intensive input from the MeA²³ mediates both acute and expected attack²⁷. Therefore, we hypothesized that the MeA OXTR neurons projecting to the AI (MeA^{OXTR+AI}) or VMHvl (MeA^{OXTR+VMHvl}) regulate consolation and aggression, respectively. Such two different pathways may also underlie the transformation of prosocial and antisocial behaviors in different social contexts.

In mandarin voles (*Microtus mandarinus*), males often display high levels of consolation to partners, but intensive aggression to

unfamiliar intruders²⁸. Using males of this species and multiple methods such as tracing strategies of viruses, apoptosis, pharmacology, fiber photometry, optogenetics, pharmacogenetics, and electrophysiology, the present study revealed the significant role of different populations of OXTR neurons in the MeA projecting to AI and VMHvl in control of consolation and aggression, respectively. The detailed experimental design and procedures are shown in Supplementary Fig. 1.

Results

Involvement of AI, VMHvl, and MeA in consolation and aggression

To test the involvement of the AI, VMHvl, and MeA in consolation and aggression, c-Fos positive neurons in the three brain regions were quantified 90 min after both the consolation test (Consolation group) and resident-intruder paradigm (Aggression group). The stress-buffering effect of allogrooming between male sibling voles was verified (detailed descriptions are displayed in Supplementary Note. 1 and Supplementary Fig. 2) and allogrooming could be considered a consolation behavior. Control subjects (CON group) and subjects whose siblings were housed separately only (without footshock) (Separation group) were assigned as control groups. As shown in Supplementary Fig. 3, the Aggression (posterior dorsal (PD) subregion: 50.49 ± 3.23 ; posterior ventral (PV) subregion: 54.38 ± 3.31) and Consolation (PD:

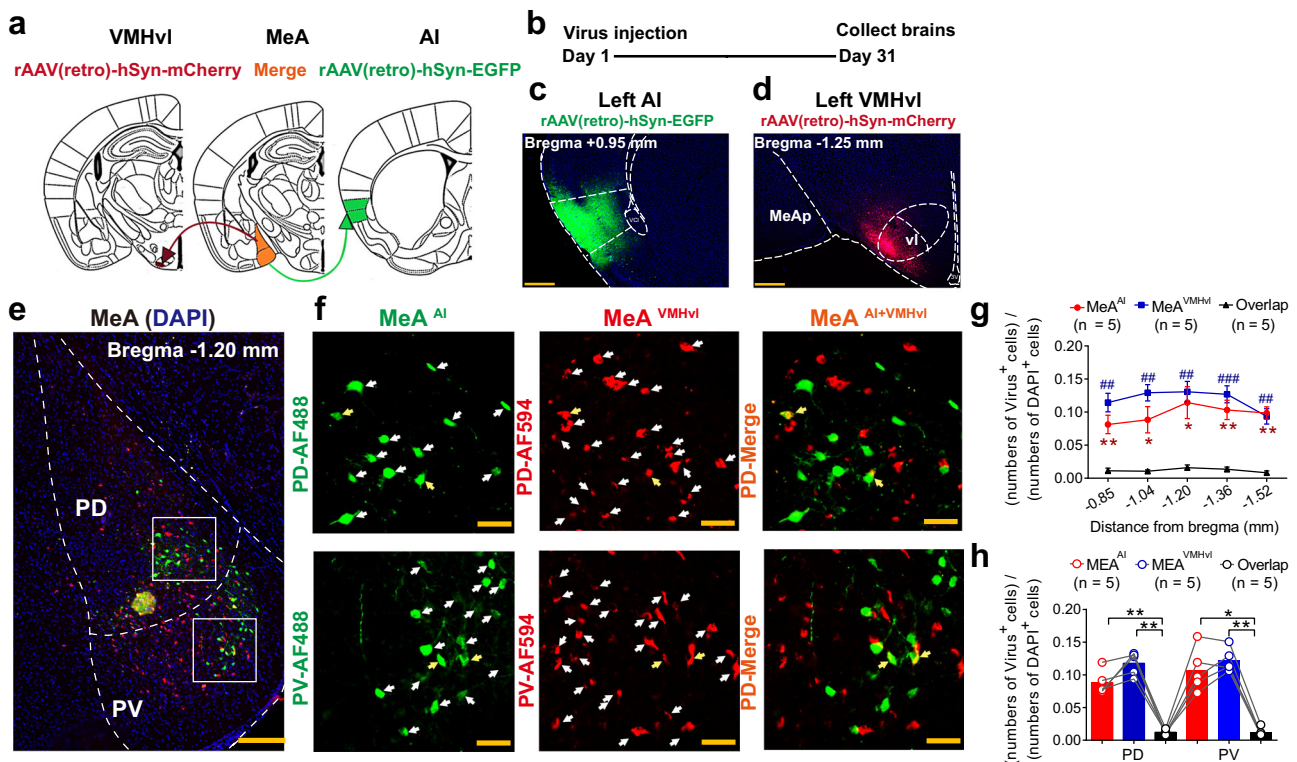


Fig. 1 | The morphological distribution of the MeA neurons projecting to the AI and VMHvl. **a, b** Diagram showing virus injection regimen (adapted from *The Mouse Brain in Stereotaxic Coordinates* by Paxinos and Franklin, **a**) and schedule (**b**). **c, d** Representative images of rAAV (retro)-mCherry (red) and rAAV (retro)-EGFP (green) injection sites at the AI (**c**) and VMHvl (**d**). Scale bars, 500 μ m. 5 independent repetitions with similar results in (**c**) and (**d**). **e, f** Representative images with retro-virus labeling at both the posterior dorsal (PD) and posterior ventral (PV) subregions of MeA. The selected boxed areas were magnified (300 μ m \times 300 μ m). The MeA^{AI} and MeA^{VMHvl} were characterized by white arrows. The MeA^{AI+VMHvl} were characterized by yellow arrows. Scale bars, 200 μ m in **e** and 50 μ m in (**f**). **g** Proportions of MeA^{AI}, MeA^{VMHvl}, MeA^{AI+VMHvl} at the MeA along the anteroposterior axis. * and # implies a discrepancy between the Overlap and MeA^{AI} / MeA^{VMHvl},

respectively. Overlap versus MeA^{AI}: $p = 0.0099, 0.0390, 0.0246, 0.0042,$ and 0.0010 at bregma $-0.85, -1.04, -1.20, -1.36,$ and -1.50 mm, respectively; Overlap versus MeA^{VMHvl}: $p = 0.0021, 0.0028, 0.0031, 0.0010$ and 0.0035 at bregma $-0.85, -1.04, -1.20, -1.36,$ and -1.50 mm, respectively. **h** Proportions of MeA^{AI}, MeA^{VMHvl}, MeA^{AI+VMHvl} at the PV and PD. At the PD subregion, MeA^{AI} versus Overlap, $p = 0.006$; MeA^{VMHvl} versus Overlap, $p = 0.003$. At the PV subregion, MeA^{AI} versus Overlap, $p = 0.021$; MeA^{VMHvl} versus Overlap, $p = 0.006$. $n = 5$ voles in (**g**) and (**h**). *** $p < 0.001$, ** $p < 0.01$, * $p < 0.05$. Data was analyzed by repeated measure two-way (**g**) and one-way (**h**) ANOVA with Sidak's multiple comparison test. Data are presented as the means \pm SEM. Statistical details are presented in Supplementary Data. 1 file. Source data are provided as a Source Data file.

45.55 ± 3.80; PV: 58.28 ± 5.98) groups showed more numbers of c-Fos positive cells than the CON (PD: 20.39 ± 1.62; PV: 23.91 ± 2.32) and the Separation groups (PD: 18.43 ± 1.22; PV: 20.69 ± 1.11) in the MeA (Supplementary Fig. 3a–d and m). In the AI, the Consolation group (49.97 ± 7.54) showed more numbers of c-Fos positive cells than the CON (21.06 ± 2.60), Separation (24.58 ± 0.42) and Aggression (30.13 ± 1.61) groups (Supplementary Fig. 3e–h and n). In the VMHvl, the Aggression group (43.03 ± 4.72) showed more numbers of c-Fos positive cells than the CON (17.33 ± 3.08), Separation (16.12 ± 0.56) and Consolation (19.13 ± 0.84) groups (Supplementary Fig. 3i–l and o). The involvements of the three regions in consolation and aggression were thus determined. Whether the MeA projects to the AI and VMHvl was the next question that needed to be answered.

Roles of MeA-AI and MeA-VMHvl in consolation and aggression

AAVs (2/R) viruses with EGFP and mCherry were used to retrograde tracing of the projections from the MeA to AI and VMHvl, respectively, in the same vole. The injection regimen, schedule, and representative micrograph of injection sites were shown in Fig. 1a–d. 30 days after injection of AAVs (2/R) viruses with different fluorescence, two populations of neurons labeled by EGFP and mCherry were obviously observed in the MeA (Fig. 1e, f). The fraction of the MeA^{AI}, MeA^{VMHvl}, and

overlapped cells were quantified along the anterior-posterior axis from bregma –0.85 to –1.52 mm (Fig. 1g and Supplementary Fig. 4a, b). Both proportions of the MeA^{AI} (posterior dorsal (PD): 8.81% ± 0.83%; posterior ventral (PV): 10.72% ± 1.49%) and MeA^{VMHvl} (PD: 11.76% ± 0.79%; PV: 12.18% ± 0.82%) are much higher than the overlapped neurons (PD: 1.22% ± 0.16%; PV: 1.22% ± 0.29%) (Fig. 1h and Supplementary Fig. 4c). The MeA^{AI} and MeA^{VMHvl} thus are mixed but not overlapped populations. The existence and distinction of morphological distribution inspired us to explore their involvement in the regulation of consolation and aggression.

To answer this question, the AI or VMHvl neurons receiving monosynaptic projections from the MeA (the AI^{MeA} or VMHvl^{MeA}) were marked by EGFP using rAAV (2/1) viral strategy (Fig. 2a, b). These two populations of neurons in subjects from the Separation group (Fig. 2c), CON group (Fig. 2d), Consolation group (Fig. 2e) and Aggression group (Fig. 2f) were labeled by c-Fos (Cy3, red). As shown in Fig. 2g–i and Supplementary Fig. 5, the Consolation group (30.17% ± 3.73%) had a higher percentage of co-labeling neurons than the Separation (9.40% ± 0.86%), CON (10.76% ± 0.32%) and Aggression (13.55% ± 1.35%) groups in the AI (Fig. 2j). The representative images with VMHvl^{MeA} (EGFP) and c-Fos co-labeling neurons were shown in Fig. 2k–m and Supplementary Fig. 6. The Aggression group (36.96% ± 4.61%) had

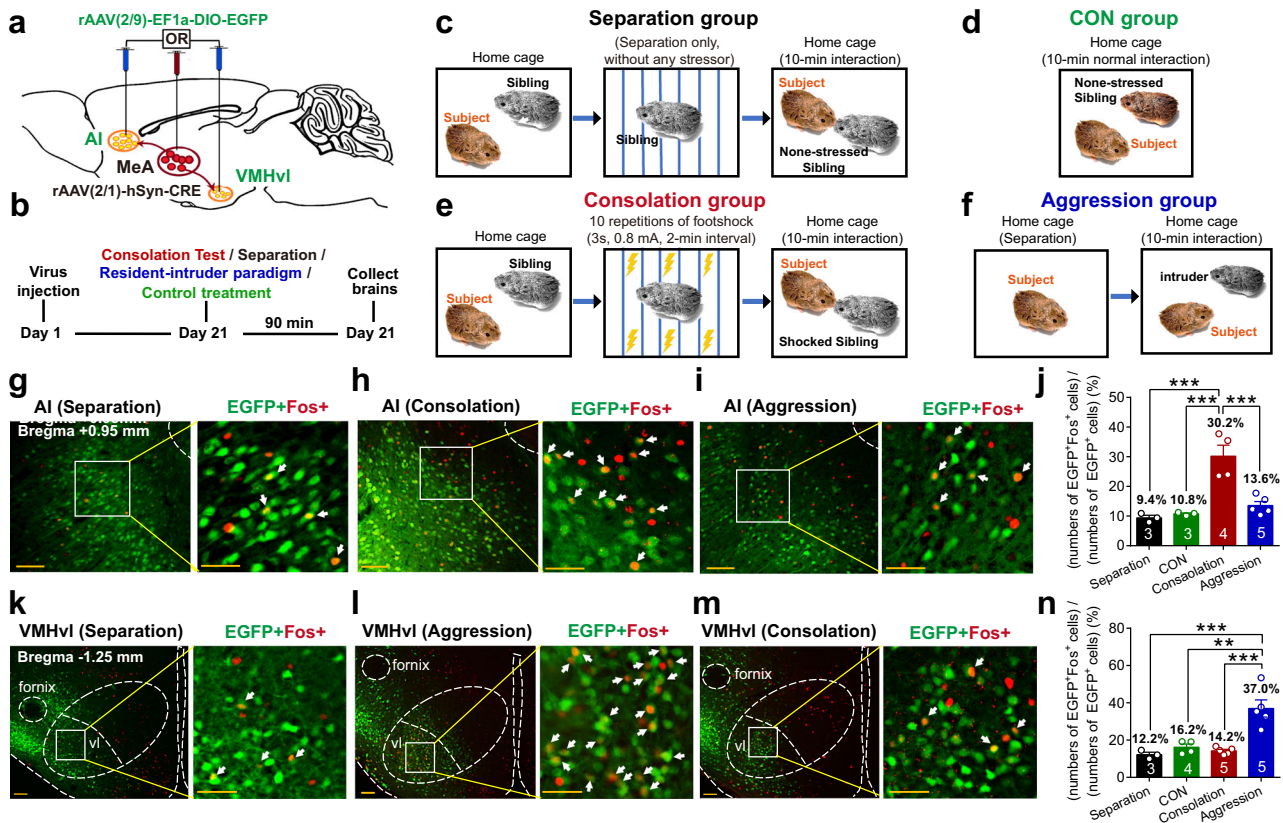


Fig. 2 | The positive involvement of MeA–AI in consolation and MeA–VMHvl in aggression, respectively. **a, b** Diagram showing injection protocol (adapted from *The Mouse Brain in Stereotaxic Coordinates* by Paxinos and Franklin, **a**) and schedule (**b**) of anterograde monosynaptic labeling virus. **c–f** Experimental process diagrams of different treatments in Separation, CON, Consolation, and Aggression groups. **g–i** Representative overlapped images of anterograde monosynaptic virus (EGFP, green) and c-Fos (Cy3, red) at the AI after separation treatment (Separation group, **g**), consolation test (Consolation group, **h**) and resident-intruder paradigm (Aggression group, **i**). **k–m** Representative overlapped images of anterograde monosynaptic virus and c-Fos at the VMHvl in Separation, Consolation, and Aggression groups. Scale bars, 100 μ m in **g–i** and **k–m**. The selected boxed areas were magnified (200 μ m \times 200 μ m) (scale bars, 50 μ m). Co-labeled neurons were

characterized by white arrows. **j, n** Comparison of percentage of EGFP and c-Fos co-labeling neurons in whole anterograde virus-marked neurons at the AI ($n = 3, 3, 4$ and 5 voles) or VMHvl ($n = 3, 4, 5$, and 5 voles) in Separation, CON, Consolation and Aggression groups, respectively. At the AI (**j**), Separation versus Consolation, $p = 0.0004$; CON versus Consolation, $p = 0.0007$; Aggression versus Consolation, $p = 0.0008$. At the VMHvl (**n**), Separation versus Aggression, $p = 0.0006$; CON versus Aggression, $p = 0.0013$; Consolation versus Aggression, $p = 0.0003$. $***p < 0.001$, $**p < 0.01$. Data was analyzed by one-way ANOVA with Sidak's multiple comparison test in **j** and **n**. Data are presented as the means \pm SEM. Statistical details are presented in Supplementary Data. 1 file. Source data are provided as a Source Data file.

higher percentage of co-labeling neurons than the Separation (12.19% ± 1.32%), CON (16.17% ± 1.70%) and Consolation groups (14.22% ± 0.82%) in the VMHvl (Fig. 2n). This result was also confirmed using fluorescent anterograde transsynaptic tracer (mWGA-mCherry) and c-Fos labeling. And very rare axon projections to the MeA were from the AI and VMHvl somata, respectively (detailed descriptions of data are displayed in Supplementary Note. 2, Supplementary Fig. 7 and Supplementary Fig. 8).

These results strongly supported the specific involvement of the MeA-AI and MeA-VMHvl in consolation and in aggression, respectively. However, it was unknown whether MeA OXTR neurons projecting to these two brain regions are involved in specific behavior via these two projections.

Necessity of MeA^{OXTR+AI} and MeA^{OXTR+VMHvl} for consolation and aggression

To explore the distribution of the MeA^{OXTR+AI} and MeA^{OXTR+VMHvl} populations, rAAV2/R-hSyn-EGFP (green) and rAAV2/R-hSyn-mCherry (red) were injected into the AI and VMHvl, respectively, in a same vole. MeA^{OXTR} neurons were labeled by OXTR antibody conjugated AF-647 (magenta) fluorescence after confirmation of the high effectiveness (97.11% ± 0.61%) and specificity (97.37% ± 0.96%) of the OXTR antibody by the co-detection strategy of Fluorescence in situ hybridization (FISH) and Immunofluorescence (IF) (Supplementary Fig. 9). The injection regimen, schedule and representative site picture were shown in Fig. 3a–d. Dual-AAVs (2/R) tracing revealed that the MeA^{OXTR+AI} had a significantly distinct morphological distribution from the MeA^{OXTR+VMHvl} along the anteroposterior axis from bregma -0.85 mm to -1.52 mm in both the posterior ventral (PV) and posterior dorsal (PD) subregions (Fig. 3e–g and Supplementary Fig. 10). On the

other hand, proportion of the MeA^{OXTR+VMHvl} in the whole VMHvl-retro cells (60.68% ± 3.18%) and proportion of the MeA^{OXTR+AI} in the whole AI-retro cells (59.32% ± 2.77%) are significantly higher than the proportion of the OXTR neurons in the whole MeA cells (33.91% ± 1.62%) (Fig. 3h). This result indicated that both the MeA^{VMHvl} and MeA^{AI} cells prefer to express OXTR.

Given the MeA^{AI} and MeA^{VMHvl} are involved in consolation and aggression, respectively (Fig. 2g–n and Supplementary Fig. 7), and the possible preference for OXTR expression in both the MeA^{AI} and MeA^{VMHvl} (Fig. 3h), and the reported involvement of MeA^{OXTR} in both pro-social and anti-social behaviors^{16,18,29,30}, whether and how OXTR regulates consolation and aggression via the MeA^{AI} and MeA^{VMHvl} are needed to be investigated.

As shown in Supplementary Fig. 11a–c, the cells infected by rAAV2/9-OXTR-mCherry virus were very restricted to neurons labeled by anti-OXTR (merged ratio: 92.15%). Neurons infected with the virus accounted for about 73.53% of the total numbers of MeA^{OXTR}. In addition, it was found that the MeA OXTR neurons had similar projections to AI and MPOA, and to BNST and VMHvl (detailed descriptions are displayed in Supplementary Note 3 and Supplementary Fig. 11d–k).

Then the apoptosis scheme was used to determine the specific necessity of the two populations of neurons on consolation and aggression. Caspase3 (Casp3) virus was used to induce apoptosis of the MeA^{OXTR+AI} and MeA^{OXTR+VMHvl} (Fig. 4a, b). As shown in Fig. 4c, d, and Supplementary Fig. 12, infection of the two neuronal populations with the Casp3 virus led to rapid Cre-dependent death of MeA^{OXTR} neurons (Fig. 4e). Apoptosis of the MeA^{OXTR+AI} significantly reduced allogrooming and sniffing to stressed siblings (Fig. 4f, g) but produced no effects on attack to intruders (Fig. 4h). In contrast, apoptosis of the MeA^{OXTR+VMHvl} significantly reduced attack (Fig. 4k) but produced no

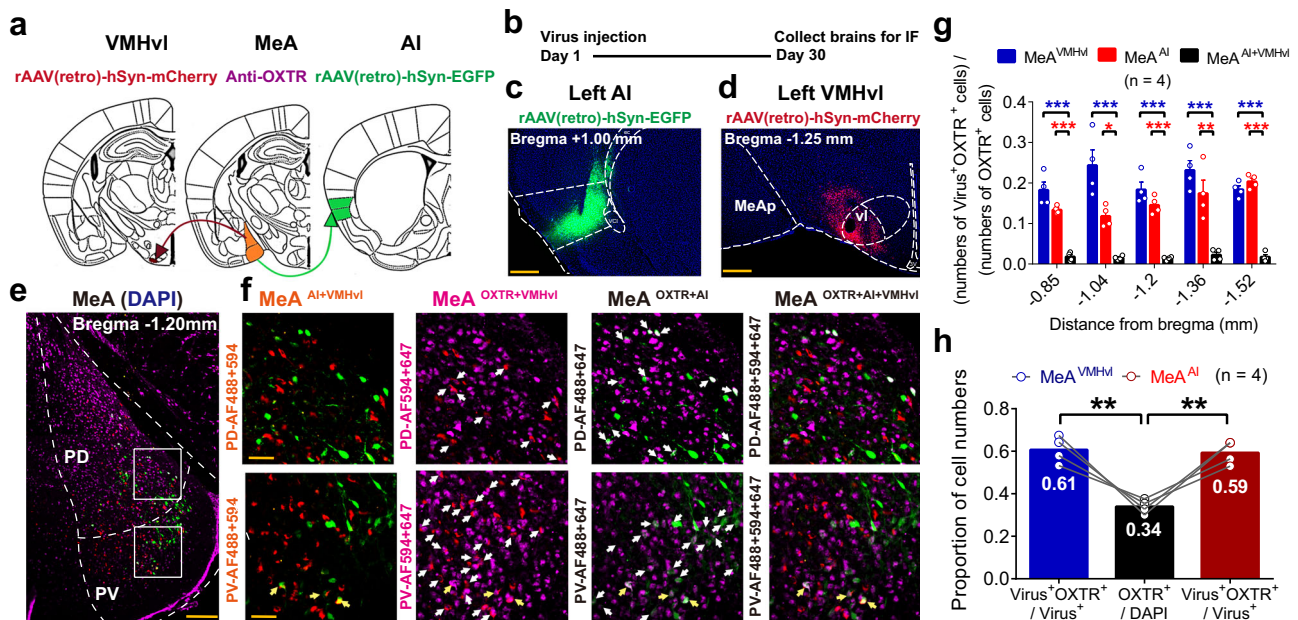


Fig. 3 | The morphological distribution of the MeA^{OXTR+AI} and MeA^{OXTR+VMHvl} populations. **a, b** Diagram showing virus injection regimen (adapted from *The Mouse Brain in Stereotaxic Coordinates* by Paxinos and Franklin, **a**) and schedule (**b**). **c, d** Representative images of rAAV-retro-mCherry (red) and rAAV-retro-EGFP (green) injection sites at the AI (**c**) and VMHvl (**d**). Scale bars, 500 μm. 4 independent repetitions with similar results in (**c**) and (**d**). **e, f** Representative overlapped images of dual-retrograde rAAVs tracing and OXTR antibody (AF647, magenta) at both PD and PV subregions (**e**). The enlarged views of the selected boxed areas (300 μm × 300 μm). **f** White arrows indicate MeA^{AI+OXTR} and MeA^{VMHvl+OXTR}. Yellow arrows indicate merged neurons (MeA^{AI+OXTR+VMHvl}). Scale bars, 200 μm (**e**) and 50 μm (**f**). **g** Proportion of different retrograde virus-positive and overlapped neurons expressing OXTR along the anteroposterior axis of the MeA.

MeA^{AI} versus MeA^{AI+VMHvl}, $p < 0.001$, $=0.036$, <0.001 , $=0.004$ and <0.001 at bregma -0.85, -1.04, -1.20, -1.36 and -1.50 mm, respectively; MeA^{VMHvl} versus MeA^{AI+VMHvl}, $p < 0.001$, <0.001 , <0.001 , <0.001 , and <0.001 at bregma -0.85, -1.04, -1.20, -1.36, and -1.50 mm, respectively. **h** Proportion of different virus-positive cells expressing OXTR and of the anti-OXTR cells in the total MeA cells. MeA^{AI} versus MeA^{Overall}, $p = 0.0017$; MeA^{VMHvl} versus MeA^{Overall}, $p = 0.0013$; $n = 4$ voles in (**g**) and (**h**). $***p < 0.001$, $**p < 0.01$, $*p < 0.05$. Data was analyzed by repeated measure two-way (**g**) and one-way (**h**) ANOVA with Sidak’s multiple comparison test. Data are presented as the means ± SEM. Statistical details are presented in Supplementary Data. 1 file. Source data are provided as a Source Data file. IF immunofluorescence experiment.

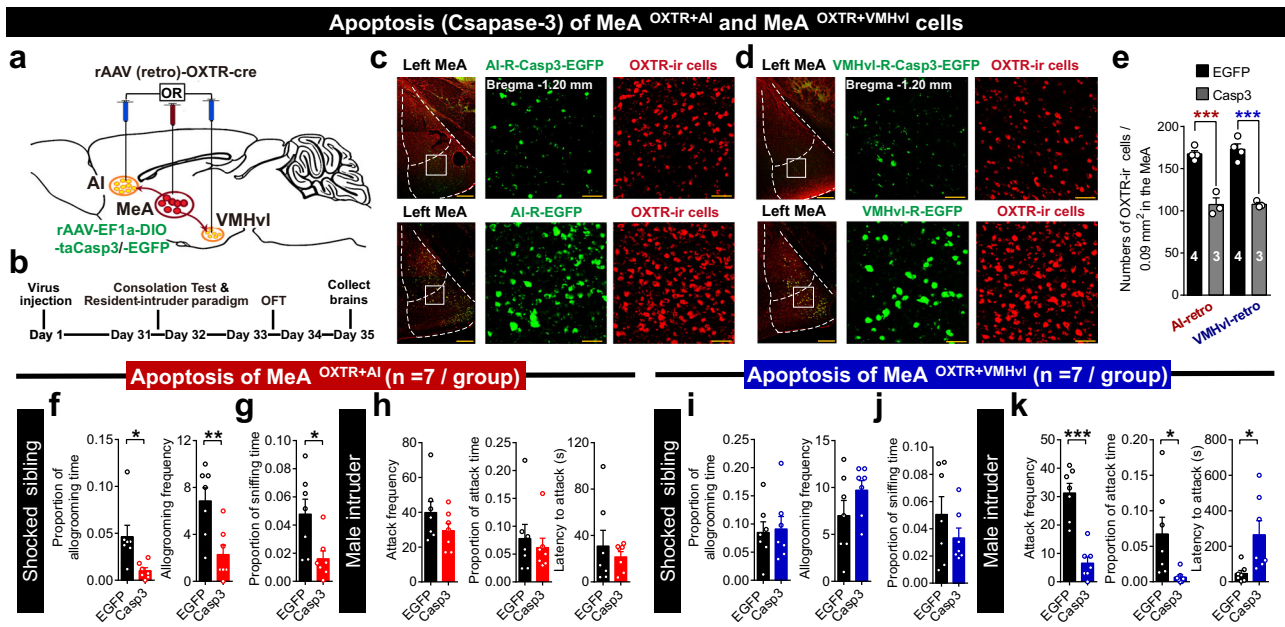


Fig. 4 | The effects of apoptosis of the MeA^{OXTR+AI} and MeA^{OXTR+VMHvl} on consolation and aggression. **a, b** Diagram showing protocol (adapted from *The Mouse Brain in Stereotaxic Coordinates* by Paxinos and Franklin, **a**) and schedule (**b**) of virus injection for apoptosis of bilateral MeA^{OXTR+AI} or MeA^{OXTR+VMHvl}. **c, d** Representative co-labeling images of AI-retro (**c**)/VMHvl-retro (**d**) Caspase3 or EGFP (green) and anti-OXTR (OXTR-ir, Cy3, red) cells in the MeA (scale bars, 200 μ m). The enlarged views of the selected boxed areas (300 μ m \times 300 μ m) (scale bars, 50 μ m). **e** Numbers of OXTR-ir cells in the MeA between AI-retro EGFP and Casp3 groups, and between VMHvl-retro EGFP and Caspase3 groups. AI-retro EGFP versus Casp3, $p = 0.0007$; VMHvl-retro EGFP versus Casp3, $p = 0.0004$. $n = 4, 3, 4$, and 3 voles in AI-retro EGFP, AI-retro Casp3, VMHvl-retro EGFP and VMHvl-retro Casp3 groups, respectively. **f, g, i, j** Duration proportion and frequency of allogrooming, and frequency of sniffing siblings between AI-retro EGFP and Casp3

groups (**f, g**), and between VMHvl-retro EGFP and Casp3 groups (**i, j**). **h, k** Frequency, duration proportion of attack, and latency to attack between the AI-retro EGFP and Casp3 groups (**h**), and between the VMHvl-retro EGFP and Casp3 groups (**k**). In **f-h**, AI-retro EGFP versus AI-retro Casp3, allogrooming time proportion: $p = 0.014$; allogrooming frequency: $p = 0.006$; sniffing time proportion: $p = 0.02$; attack frequency: $p = 0.196$; attack time proportion: $p = 0.533$; latency to attack: $p = 0.532$. In **i-k**, VMHvl-retro EGFP versus VMHvl-retro Casp3, allogrooming time proportion: $p = 0.278$; allogrooming frequency: $p = 0.181$; sniffing time proportion: $p = 0.278$; attack frequency: $p < 0.001$; attack time proportion: $p = 0.042$; latency to attack: $p = 0.033$. $n = 7$ voles/group in **f-k**. $^{***}p < 0.001$, $^{**}p < 0.01$, $^{*}p < 0.05$. Data was analyzed by two-tailed unpaired t -test (**e**) and paired t -test (**f-k**). Data are presented as the means \pm SEM. Statistical details are presented in Supplementary Data. 1 file. Source data are provided as a Source Data file.

effects on consolation behaviors (Fig. 4i, j). Apoptosis of the MeA^{OXTR+AI} and MeA^{OXTR+VMHvl} did not affect time (%) spent in the center and total distance in the 5-min OFT (Supplementary Fig. 13). In addition, male stressed siblings (demonstrators) showed no differences in levels of allogrooming and sniffing between AI (VMHvl)-EGFP groups and AI (VMHvl)-Casp3 group when encountering subjects (Supplementary Fig. 14a-j). The allogrooming performance of male siblings did not affect the levels of consoling behavior among subjects (Supplementary Fig. 14k-n).

For blocking OXTR functions located in the MeA, the OXTR-Antagonist (OXTA, [d (CH2) 5I, Tyr (Me) 2, Thr4, Orn8, des-Gly-NH29]-Vasotocin trifluoroacetate salt, 0.5 ng/200 nl per side) was injected to the bilateral MeA among subjects, and their consolation and aggression behaviors were then evaluated (Supplementary Fig. 15a-c). As shown in Supplementary Fig. 15d-j, both levels of consoling and aggressive behaviors were reduced after OXTA injection in the MeA.

These results strongly supported that the OXTR signaling in the MeA, and MeA^{OXTR+AI}, and MeA^{OXTR+VMHvl} neurons were necessary for the direct regulation of consolation and aggression, respectively.

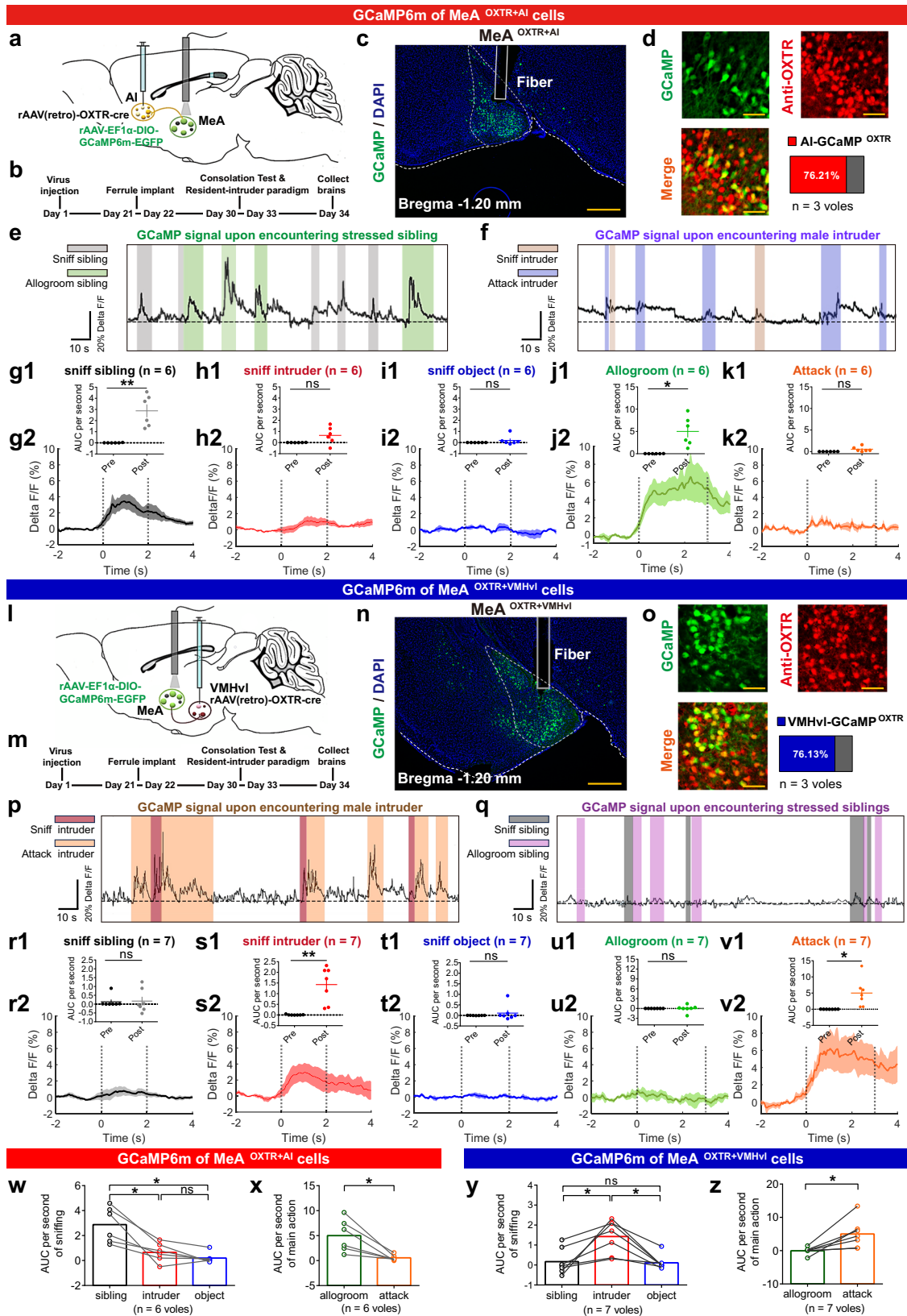
MeA OXT release and PVN^{OXT+MeA} neuron activity upon consoling and attacking

OXT sensor virus was used to detect real-time OXT release in the MeA and GCaMP6m virus was used to detect real-time activities of the PVN^{OXT+MeA}. The injection regimen, schedule, and representative site picture are shown in Supplementary Fig. 16a-c and i-k, and Supplementary Fig. 17a-c and s-u. The PVN^{OXT+MeA} GCaMP6m/EGFP neurons

(green) were relatively restricted to anti-OXT labeled cells (Cy3, red) (Supplementary Fig. 16l and Supplementary Fig. 17v). After sufficient recovery, subject voles were successively assigned to the consolation test, resident-intruder paradigm and new object recognition.

As shown in delta F/F (%) and comparison between pre-phase and post-phase AUC per second during different social behaviors, fluorescence changes of the MeA^{OXT sensor} and calcium signal of GCaMP-PVN^{OXT+MeA} showed significant increases upon sniffing sibling and intruder, allogrooming and attacking, but did not change upon sniffing object (Supplementary Fig. 16d1-h2 and m1-q2). In addition, the post-phase AUC per second of sniffing siblings and intruders was higher than that of sniffing objects. However, there was no difference in post-phase AUC per second between the sniffing sibling and sniffing intruder, and between allogrooming and attack both in the MeA^{OXT sensor} and GCaMP-PVN^{OXT+MeA} (Supplementary Fig. 16r-u). These results not only demonstrated the strong involvement of the OXT system at the MeA in the occurrence of consolation and aggression but also proposed a hypothesis that MeA^{OXT} neurons may specifically be involved in consolation or aggression by projecting to distinct target regions such as the AI or VMHvl.

The MeA^{OXT (mut)} and EGFP-PVN^{OXT+MeA} did not display changes in fluorescent signals during both social and non-social behaviors under the two tests (Supplementary Fig. 17d-r and w-k). In addition, fluorescent signals of the MeA^{OXT sensor} and GCaMP-PVN^{OXT+MeA} had no significant changes while subjects engaged in non-social behavior such as freezing, (self) grooming, exploring, and rearing during consolation test and resident-intruder paradigm (Supplementary Fig. 18).



Activities of MeA^{OXTR+AI} and MeA^{OXTR+VMHvl} upon consoling and attacking

Real-time activities of the MeA^{OXTR+AI} and MeA^{OXTR+VMHvl} populations were examined with GCaMP6m virus measured by fiber photometry. The injection regimen, schedule, representative images, and specificity

of virus infection were shown in Fig. 5a–d and l–o; Supplementary Fig. 19a–d and t–w.

The calcium signal of the MeA^{OXTR+AI} population displayed a significant increase while facing stressed siblings, but did not change while facing male intruders (Fig. 5e–k2). On the contrary, the calcium

Fig. 5 | Dynamics of GCaMP6m-fluorescence signal in the MeA^{OXTR+AI} and MeA^{OXTR+VMHvl} during social behaviors. **a, b, l, m** Virus regimen (adapted from *The Mouse Brain in Stereotaxic Coordinates* by Paxinos and Franklin, **a, l**) and schedule (**b, m**). **c, n** Images of GCaMP6m of MeA^{OXTR+AI(VMHvl)} and actual fiber tracts (scale bars, 500 μ m). 6 and 7 independent repetitions with similar results in (**c**) and (**n**). **d, o** Overlapped images of GCaMP6m (EGFP, green) and OXTR (Cy3, red) in the MeA^{OXTR+AI(VMHvl)} (scale bars, 50 μ m). $n = 3$ voles/group. **e, f, p, q** Representative traces of calcium signal in the MeA^{OXTR+AI(VMHvl)} when facing stressed siblings and male intruders. **g1–k1, r1–v1** Changes of calcium signals in the MeA^{OXTR+AI(VMHvl)} before and after sniffing siblings (**g1, p < 0.05; r1**), intruder (**h1; s1, p < 0.01**) and object (**i1; t1**), allogroom (**j1, p = 0.013; u1**) and attack (**k1; v1, p = 0.022**). **g2–k2, r2–v2** Peri-event plot of calcium signal (Delta F/F, %) in the MeA^{OXTR+AI(VMHvl)} aligned to onsets of social behaviors. Colored lines indicate group averages of 6-s calcium

signal and shaded areas indicate S.E.M. Dotted lines define time windows for analyzing AUC per second of a single event. **w–z** AUC per second distinctions of calcium signal traces in the MeA^{OXTR+AI(VMHvl)}. GCaMP6m of MeA^{OXTR+AI}, sniffing: sibling versus intruder, $p = 0.029$; sibling versus object, $p = 0.015$. Allogrooming versus attack, $p = 0.015$. GCaMP6m of MeA^{OXTR+VMHvl}, sniffing: sibling versus intruder, $p = 0.041$; intruder versus object, $p = 0.014$. Attack versus allogrooming, $p = 0.018$. $n = 6$ and 7 voles in (**w, x**) and (**y, z**). Data was analyzed by a two-tail paired t -test (**g1–k1, r1–v1, x, z**) and Repeated measure one-way ANOVA with Sidak's multiple comparison test (**w, y**). $^{**}p < 0.01$, $^{*}p < 0.05$. Data are presented as the means \pm SEM. Statistical details are presented in Supplementary Data.1 file. Source data are provided as a Source Data file. AUC area under the curve, Delta F/F (%) change in fluorescence as a function of baseline fluorescence, ns no significance.

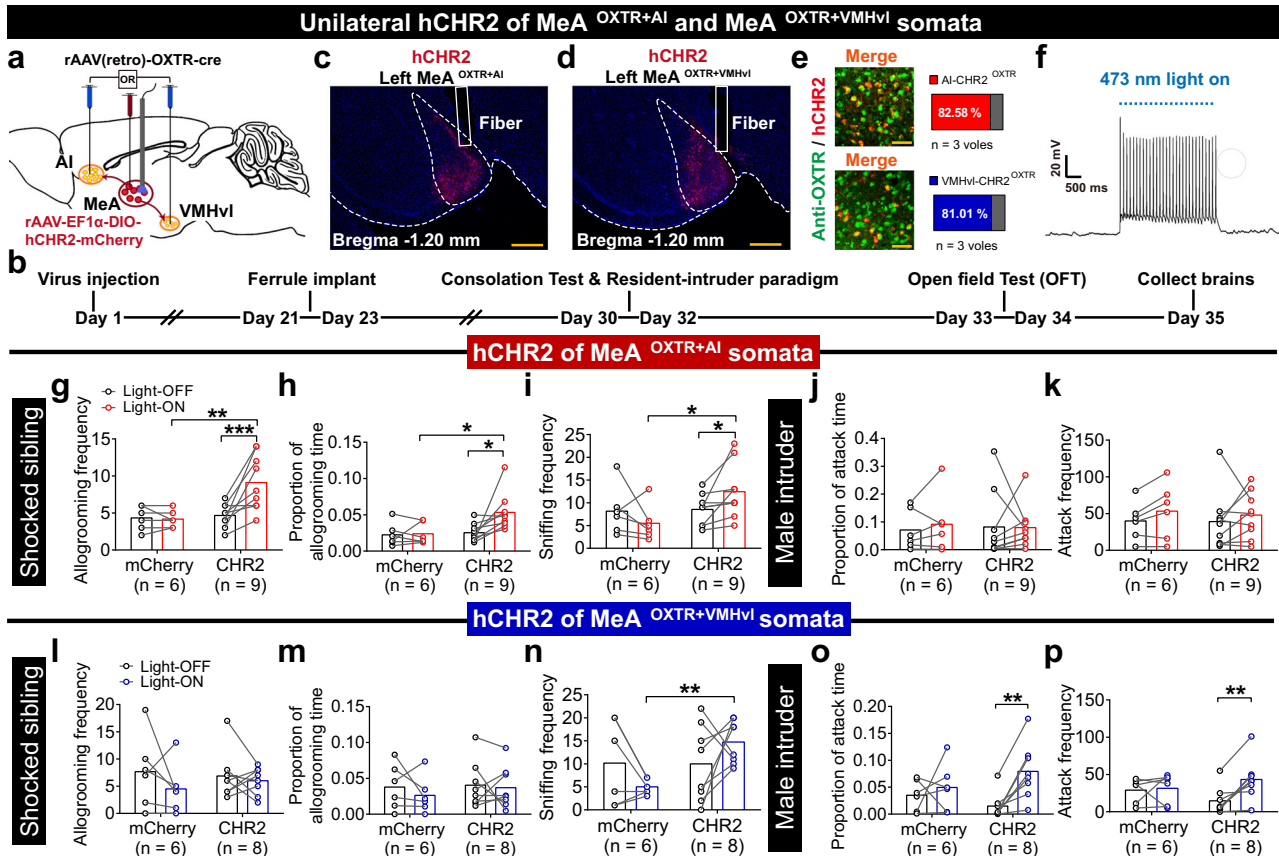


Fig. 6 | Effects of optogenetic activation of MeA^{OXTR+AI} and MeA^{OXTR+VMHvl} somata on consoling and aggression. **a, b** Virus regimen (adapted from *The Mouse Brain in Stereotaxic Coordinates* by Paxinos and Franklin, **a**) and schedule (**b**) for optogenetic activation of the somata. **c, d** Images of OXTR-hCHR2 expression (mCherry, red) in the MeA^{OXTR+AI} and MeA^{OXTR+VMHvl} (scale bars, 500 μ m). 9 and 8 independent repetitions with similar results in (**c**) and (**d**). **e** Overlapped images of hCHR2 (mCherry) and anti-OXTR (AF488, green) cells in the MeA^{OXTR+AI} and MeA^{OXTR+VMHvl} (scale bars, 50 μ m). $n = 3$ voles/group. **f** Representative trace from electrophysiological recordings showing photoactivation of the MeA^{OXTR+AI} or MeA^{OXTR+VMHvl} soma. **g–k** Comparison of allogrooming and sniffing siblings, and of attacking intruders between the AI-retro CHR2 and mCherry groups. n (mCherry) = 6 voles; n (CHR2) = 9 voles. Allogrooming frequency: CHR2-Light OFF versus CHR2-Light ON, $p < 0.001$; mCherry-Light ON versus CHR2-Light ON, $p = 0.008$; Allogrooming time

proportion: CHR2-Light OFF versus CHR2-Light ON, $p = 0.026$; mCherry-Light ON versus CHR2-Light ON, $p = 0.026$; sniffing frequency: CHR2-Light OFF versus CHR2-Light ON, $p = 0.040$; mCherry-Light ON versus CHR2-Light ON, $p = 0.027$. **l–p** Comparison of allogrooming and sniffing siblings, and of attacking intruders between the VMHvl-retro CHR2 and mCherry groups. n (mCherry) = 6 voles, n (CHR2) = 8 voles. Sniffing frequency: mCherry-Light ON versus CHR2-Light ON, $p < 0.001$; attack time proportion: CHR2-Light OFF versus CHR2-Light ON, $p = 0.002$; attack frequency: CHR2-Light OFF versus CHR2-Light ON, $p = 0.002$. Data was analyzed by repeated measure two-way ANOVA with Sidak's multiple comparison test (**g–p**). $^{***}p < 0.001$, $^{**}p < 0.01$, $^{*}p < 0.05$. Data are presented as the means \pm SEM. Statistical details are presented in Supplementary Data.1 file. Source data are provided as a Source Data file.

signal of the MeA^{OXTR+VMHvl} showed significant changes while facing male intruders, but did not change while facing stressed siblings (Fig. 5p–v2). Post-phase AUC per second of the MeA^{OXTR+AI} was higher while sniffing siblings than sniffing intruders and objects, and was higher while allogrooming than attacking (Fig. 5w, x). But post-phase AUC per second of the MeA^{OXTR+VMHvl} was higher while sniffing intruders

than sniffing sibling and object, and was higher while attacking than allogrooming (Fig. 5y, z). Such a phenomenon demonstrated the above-mentioned hypothesis that the MeA^{OXTR+AI} and MeA^{OXTR+VMHvl} were involved in consoling and aggression, respectively.

The EGFP-MeA^{OXTR+AI} and EGFP-MeA^{OXTR+VMHvl} (Supplementary Fig. 19e–s and x–l') did not display changes in fluorescent signals

during both social and non-social behaviors under the two tests. In addition, fluorescent signals of the GCaMP-MeA^{OxTR+AI} and GCaMP-MeA^{OxTR+VMHvl} had no significant changes while subjects engaged in non-social behavior during two tests (Supplementary Fig. 20). These results of control experiments validated the measurement of OXT release and neuron activities utilizing fluorescent signals by infecting specific neurons using sensor or GCaMP AAVs.

To verify the specific activation of the two populations under consolation and aggression, we performed triple labeling of anti-c-Fos (Cy3, red), anti-OXTR (AF405, magenta) and AAV(2/R)-EGFP (green) tracing in voles exhibited allogrooming or attack (Supplementary Fig. 21a–c and j–l). The fractions of the activated MeA^{OxTR+AI} and MeA^{OxTR+VMHvl} under separation treatment, house-group treatment, consolation, and aggression (Supplementary Fig. 21d–f and m–o) were quantified along the anterior-posterior axis from bregma –0.85 mm to –1.52 mm (Supplementary Fig. 21g and p). Approximately 36.81% of the MeA^{OxTR+AI} and 45.26% of the MeA^{OxTR+VMHvl} neurons were activated by consolation and aggression, respectively. The activated ratios under consolation and aggression were significantly higher than the level under control (MeA^{OxTR+AI}: 14.16%; MeA^{OxTR+VMHvl}: 17.73%) and separation

treatment (MeA^{OxTR+AI}: 16.98%; MeA^{OxTR+VMHvl}: 20.83%) (Supplementary Fig. 21h and q). Both the posterior ventral and posterior dorsal subregions showed higher activity under consolation and aggression (Supplementary Fig. 21i and r). These results demonstrated the above fiber photometric results and revealed the morphological distribution of the recruited MeA^{OxTR+AI} population under consolation and the recruited MeA^{OxTR+VMHvl} population under aggression.

Activation of somata or fibers of the MeA^{OxTR+AI} and MeA^{OxTR+VMHvl} promotes consolation and aggression, respectively

For optogenetic activation of these two populations of neurons, the rAAV-EF1a-DIO-hCHR2-mCherry / rAAV-EF1a-DIO-mCherry were injected within the MeA, and rAAV(retro)-OXTR-cre were injected to the AI or VMHvl unilaterally (Fig. 6a and Supplementary Fig. 22a; Fig. 7a and Supplementary Fig. 23a). 7-day recovery after implantation of optic fiber, the consolation test and resident-intruder paradigm were introduced to evaluate the behavioral changes following stimulation of CHR2 with intermittent 473-nm LED in somata and fibers (Figs. 6b and 7b). The representative images of virus expression in the MeA were shown in Fig. 6c, d, Supplementary Fig. 22b, c, Fig. 7c, d and

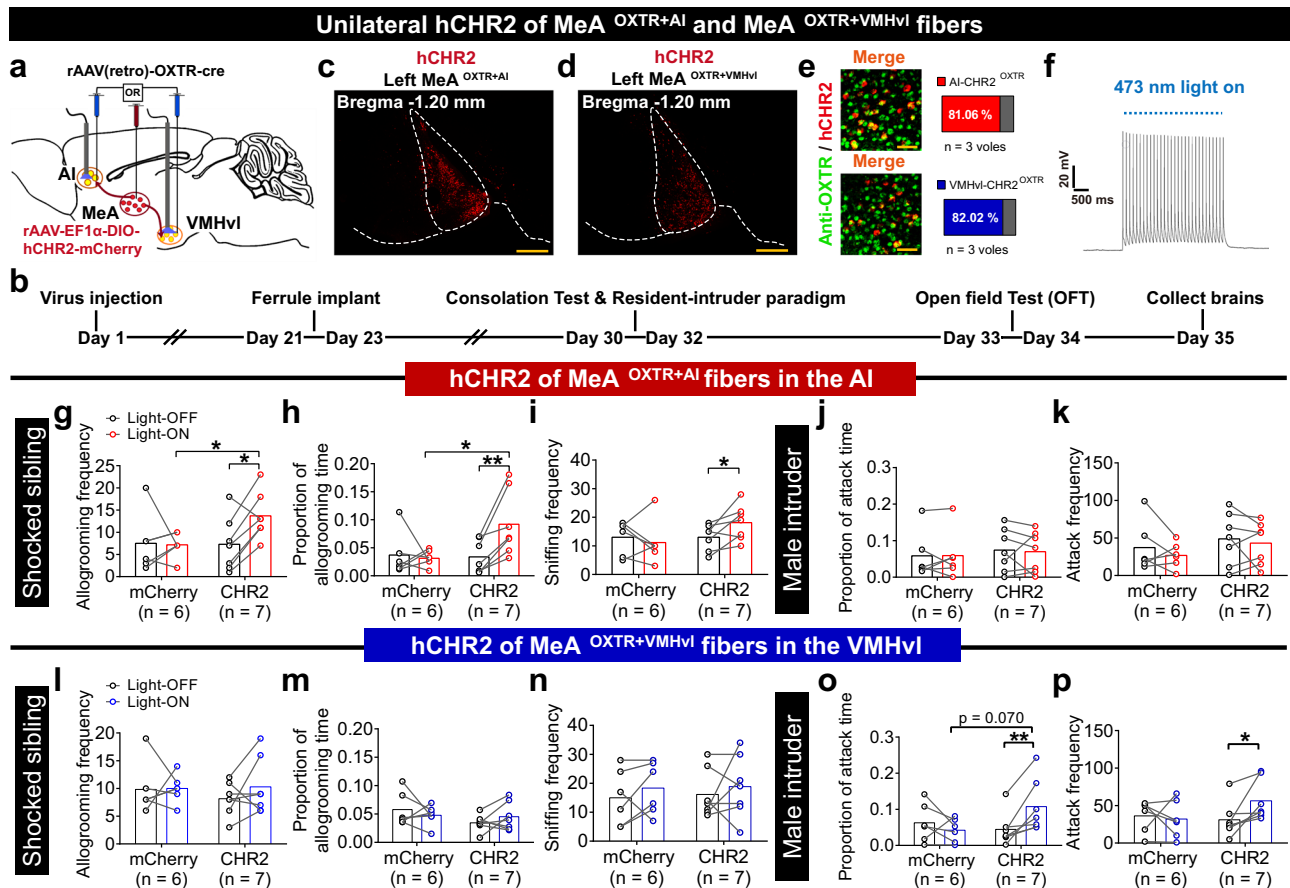


Fig. 7 | Effects of optogenetic activation of MeA^{OxTR+AI} and MeA^{OxTR+VMHvl} fibers on consolation and aggression. **a**, b Virus regimen (adapted from *The Mouse Brain in Stereotaxic Coordinates* by Paxinos and Franklin, **a**) and schedule (**b**) for optogenetic activation of the fibers. **c, d** Images of OXTR-hCHR2 expression (mCherry, red) in MeA^{OxTR+AI} and MeA^{OxTR+VMHvl} (scale bars, 500 μm). 7 independent repetitions with similar results in **(c)** and **(d)**. **e** Overlapped images of hCHR2 (mCherry) and anti-OXTR (AF488, green) cells in the MeA^{OxTR+AI} and MeA^{OxTR+VMHvl} (scale bars, 50 μm). *n* = 3 voles/group. **f** Representative traces from electrophysiological recordings showing photoactivation of the MeA^{OxTR+AI} or MeA^{OxTR+VMHvl} somata. **g–k** Comparison of allogrooming and sniffing siblings, and of attacking intruders between the AI-retro CHR2 and mCherry groups. *n* (mCherry) = 6 voles; *n* (CHR2) = 7 voles. In **g–k**, allogrooming frequency: CHR2-Light OFF versus CHR2-

Light ON, *p* = 0.0195; mCherry-Light ON versus CHR2-Light ON, *p* = 0.0158; allogrooming time proportion: CHR2-Light OFF versus CHR2-Light ON, *p* = 0.004; mCherry-Light ON versus CHR2-Light ON, *p* = 0.031; sniffing frequency: CHR2-Light OFF versus CHR2-Light ON, *p* = 0.0375. **l–p** Comparison of allogrooming and sniffing siblings, and of attacking intruders between the VMHvl-retro CHR2 and mCherry groups. *n* (mCherry) = 6 voles, *n* (CHR2) = 7 voles. In **l–p**, attack time proportion: CHR2-Light OFF versus CHR2-Light ON, *p* = 0.006; attack frequency: CHR2-Light OFF versus CHR2-Light ON, *p* = 0.0321. Data was analyzed by Repeated measure two-way ANOVA with Sidak’s multiple comparison test (**g–p**). ****p* < 0.001, ***p* < 0.01, **p* < 0.05. Data are presented as the means ± SEM. Statistical details are presented in Supplementary Data. 1 file. Source data are provided as a Source Data file.

Supplementary Fig. 23b, c. Specificity of hCHR2 and mCherry virus infection in MeA^{OXTR+AI} and MeA^{OXTR+VMHvl} were shown in Fig. 6e, Supplementary Fig. 22i, Fig. 7e and Supplementary Fig. 23i. Figure 6f and Fig. 7f showed a higher firing rate during optical 473-nm LED stimulation. Individual channels' images for representative overlapped images of anti-OXTR and hCHR2 (mCherry)-MeA^{OXTR+AI(VMHvl)} cells of activating both somata and axon fibers were shown in Supplementary Fig. 22h, i and Supplementary Fig. 23h, i, respectively. Representative merged images of axon projections and fiber trails in optogenetic experiments were also shown in Supplementary Fig. 23j-m.

Optogenetic activation of both the MeA^{OXTR+AI} somata and fibers increased allogrooming and sniffing to stressed siblings (Figs. 6g-i and 7g-i; and Supplementary Movie. 1 and Supplementary Movie. 2), but did not affect aggressive behaviors in male intruder (Fig. 6j, k and Fig. 7j, k). In contrast, optogenetic activation of both the MeA^{OXTR+VMHvl} somata and fibers increased attacks to male intruders (Figs. 6o, p and 7o, p; and Supplementary Movie 3 and Supplementary Movie 4), but did not affect consolation behaviors (Figs. 6l-n and 7l-n). The higher sniffing frequency to stressed siblings under activation of the MeA^{OXTR+VMHvl} somata may be due to the activation of other MeA^{OXTR} populations that

overlapped with the MeA^{OXTR+VMHvl} (Fig. 6n). In addition, 473-nm LED stimulation of both somata (Supplementary Fig. 22d-g) and fibers (Supplementary Fig. 23d-g) of the MeA^{OXTR+AI} or MeA^{OXTR+VMHvl} caused no changes of behavioral performance in OFT.

Inhibition of the MeA^{OXTR+AI} and MeA^{OXTR+VMHvl} decreases consolation and aggression, respectively

For pharmacogenetic inhibition of these two populations of neurons, rAAV-EF1a-DIO-hM4D(Gi)-mCherry/rAAV-EF1a-DIO-mCherry were injected within the MeA, and rAAV(retro)-OXTR-cre were injected to the AI or VMHvl bilaterally (Fig. 8a, b and Supplementary Fig. 24a). Representative images of virus infection and firing rate after pharmacogenetic inhibition (10 μM CNO infusion) are both displayed (Fig. 8c, d and f; and Supplementary Fig. 24b, c). Specificity of Gi and mCherry virus infection in MeA^{OXTR+AI} and MeA^{OXTR+VMHvl} were shown in Fig. 8e and Supplementary Fig. 24i. Individual channels' images for representative overlapped images of Gi-MeA^{OXTR+AI(VMHvl)} and anti-OXTR cells were shown in Supplementary Fig. 24h, i.

Pharmacogenetic inhibition of the MeA^{OXTR+AI} neurons significantly decreased allogrooming and sniffing to stressed siblings (Fig. 8g-i), but did not affect attack behaviors (Fig. 8j, k). In contrast,

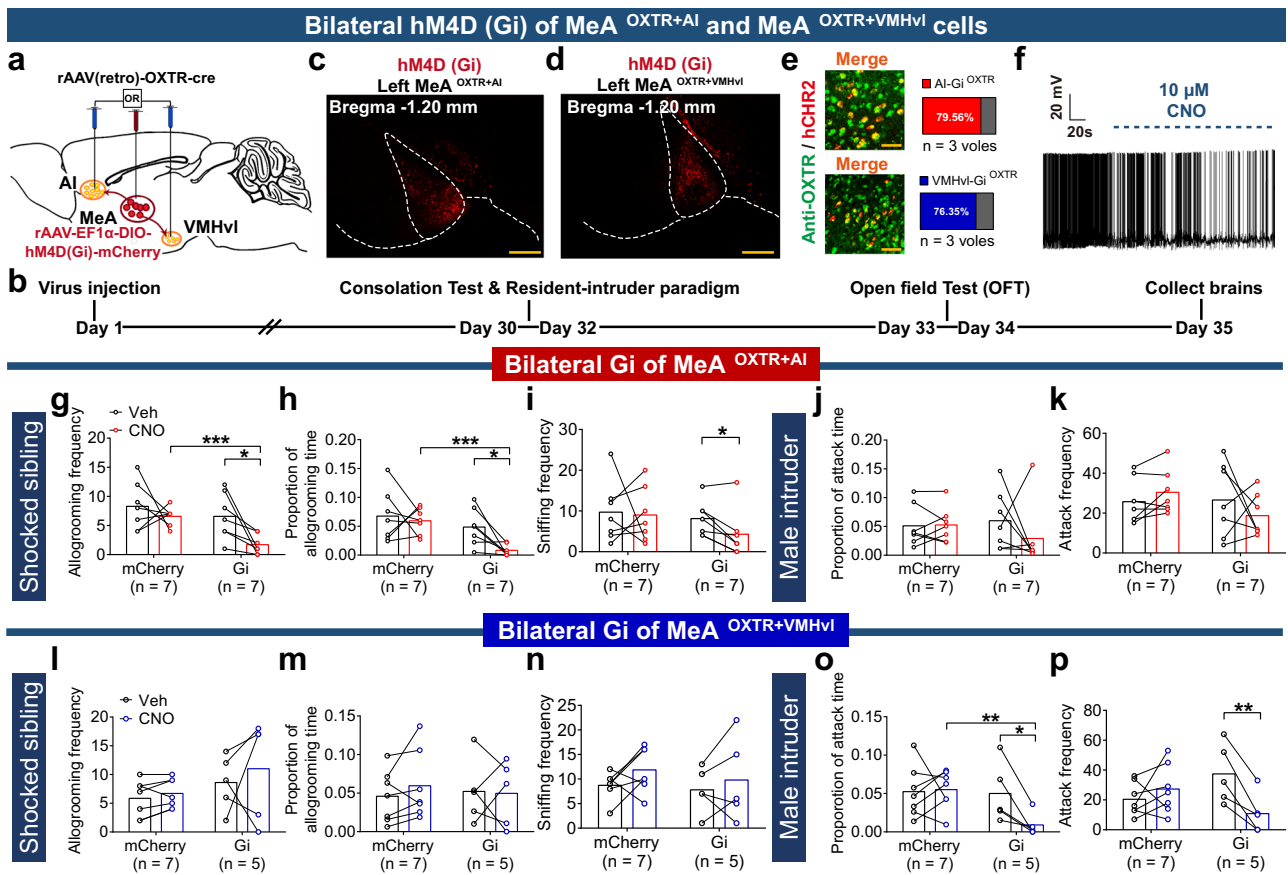


Fig. 8 | Effects of pharmacogenetic inhibition of the MeA^{OXTR+AI} and MeA^{OXTR+VMHvl} on consolation and aggression. a, b Virus regimen (adapted from *The Mouse Brain in Stereotaxic Coordinates* by Paxinos and Franklin, **a**) and schedule (**b**) for pharmacogenetic inhibition of the MeA^{OXTR+AI} and MeA^{OXTR+VMHvl}. **c, d** Images of OXTR-hM4D(Gi)-mCherry (red) expression in the MeA^{OXTR+AI} (**c**) and MeA^{OXTR+VMHvl} (**d**). Scale bars, 500 μm. 7 independent repetitions with similar results in (**c**) and (**d**). **e** Overlapped images of OXTR-Gi-mCherry and anti-OXTR (AF488, green) in the MeA^{OXTR+AI} and MeA^{OXTR+VMHvl} (scale bars, 50 μm). n = 3 voles/group. **f** Representative traces from pharmacogenetic inhibition of the MeA^{OXTR+AI} or MeA^{OXTR+VMHvl}. **g-k, l-p** Comparison of allogrooming and sniffing siblings, and of attacking intruders between the Gi and mCherry groups in the MeA^{OXTR+AI} (**g-k**) and MeA^{OXTR+VMHvl} (**l-p**). n (mCherry) = 7 voles, n (Gi) = 7 voles in (**g-k**). n (mCherry) = 7

voles, n (Gi) = 5 voles in **l-p**. In **g-k**, allogrooming frequency: Gi-saline versus Gi-CNO, *p* = 0.0243; mCherry-CNO versus Gi-CNO, *p* < 0.001; allogrooming time proportion: Gi-saline versus Gi-CNO, *p* = 0.020; mCherry-CNO versus Gi-CNO, *p* < 0.001; sniffing frequency: Gi-saline versus Gi-CNO, *p* = 0.015. In **l-p**, attack time proportion: Gi-saline versus Gi-CNO, *p* = 0.0327; mCherry-CNO versus Gi-CNO, *p* = 0.008; attack frequency: Gi-saline versus Gi-CNO, *p* = 0.003; mCherry-CNO versus Gi-CNO, *p* = 0.098. Data was analyzed by Repeated measure two-way ANOVA with Sidak's multiple comparison test (**g-p**). ***p* < 0.01, **p* < 0.05. Data are presented as the means ± SEM. Statistical details are presented in Supplementary Data. 1 file. Source data are provided as a Source Data file. Veh Vehicle (saline), CNO clozapine N-oxide.

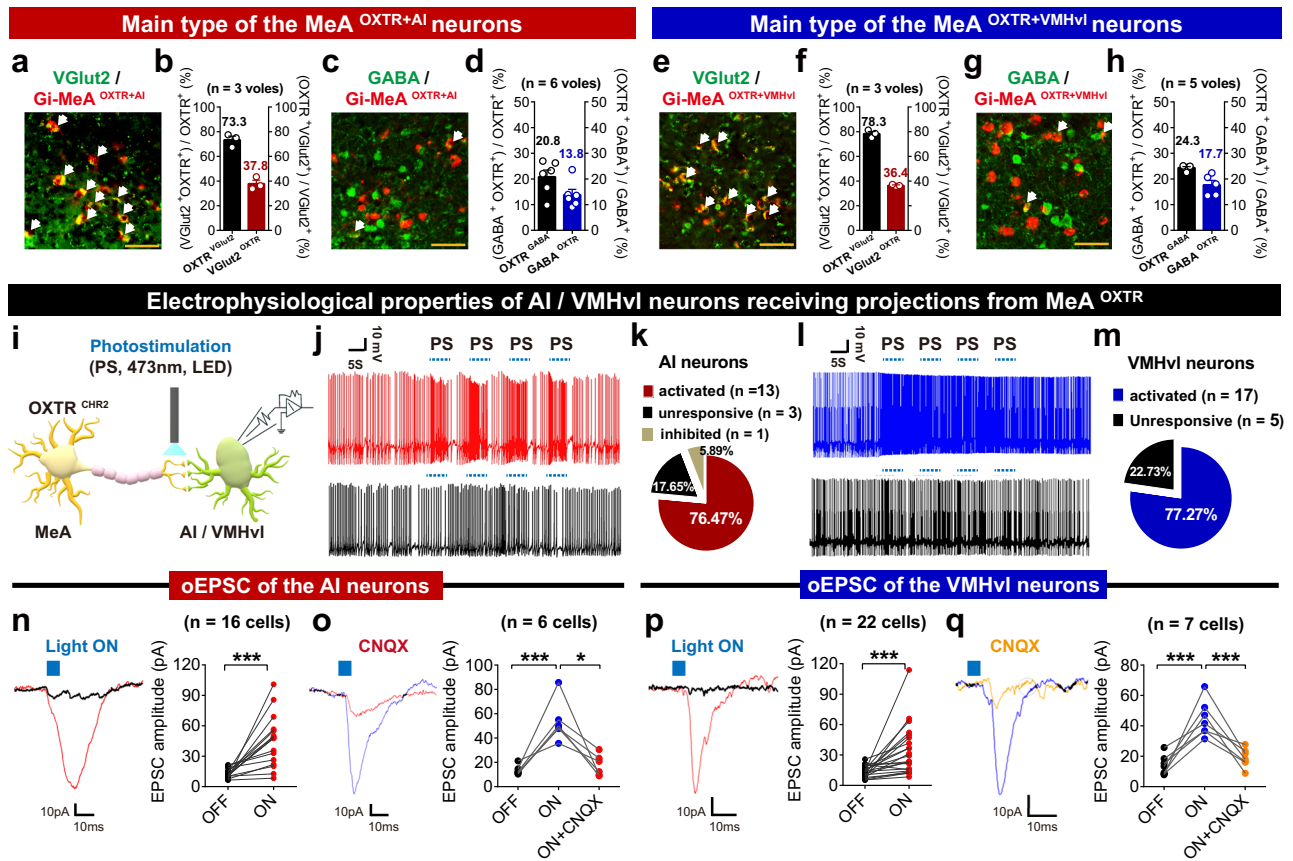


Fig. 9 | Electrophysiological characteristics of the AI and VMHvl neurons receiving monosynaptic projections from the MeA $OXTR$ neurons.

a, c, e, g Overlapped images of hM4D (Gi) (mCherry, red) and $VGlu2$ positive (AF488, green) neurons, and Gi and GABA positive (AF488, green) neurons in the MeA $^{OXTR+AI}$ (**a, c**) and MeA $^{OXTR+VMHvl}$ (**e, g**). Scale bars, 50 μm . **b, d, f, h** Quantification of the percentage of $VGlu2$ (GABA)-expressing Gi neurons and Gi-expressing $VGlu2$ (GABA) neurons in the MeA $^{OXTR+AI}$ (**b, d**) and MeA $^{OXTR+VMHvl}$ (**f, h**). $n = 3$ voles in (**b**) and (**f**), 6 voles in (**d**) and 5 voles in (**h**). **i** Experimental regimen showing photostimulation (PS) site and electrophysiological recording. **j, l** Representative activated and unresponsive spontaneous discharge rate traces under PS (**j, l**). Pie charts showing the percentage of activated neurons in the AI ($n = 17$ cells, **k**) and VMHvl ($n = 22$ cells, **m**). **n, p** EPSC traces under PS, and quantified activated effect in

the AI ($n = 16$ cells, **n**) and VMHvl ($n = 22$ cells, **p**). In (**n**), OFF versus ON, $p = 0.0002$; In (**p**), OFF versus ON, $p = 0.0007$. **o, q** EPSC traces under PS with CNQX, and quantified inhibited effect in the AI ($n = 6$ cells, **o**) and VMHvl ($n = 7$ cells, **q**). In (**o**), OFF versus ON, $p = 0.009$; ON versus ON + CNQX, $p = 0.029$; In (**q**), OFF versus ON, $p = 0.009$; ON versus ON + CNQX, $p = 0.006$. Data was analyzed by two-tail paired t -test (**n, p**) and Repeated measure one-way ANOVA with Sidak's multiple comparison test (**o, q**). $^{***}p < 0.001$, $^{*}p < 0.05$. Data are presented as the means \pm SEM. Statistical details are presented in Supplementary Data. 1 file. Source data are provided as a Source Data file. PS photostimulation, oEPSC optically evoked excitatory postsynaptic current, CNQX 6-cyano-7-nitroquinoxaline-2,3-dione (AMPA receptor antagonist).

pharmacogenetic inhibition of MeA $^{OXTR+VMHvl}$ neurons significantly decreased aggression to male intruders (Fig. 8l–n), but did not affect consolation to stressed siblings (Fig. 8o, p). In addition, pharmacogenetic inhibition of the MeA $^{OXTR+AI}$ or MeA $^{OXTR+VMHvl}$ neurons did not alter behavioral performance in OFT (Supplementary Fig. 24d–g).

Taking data of both the optogenetics and chemical genetics together, activation of the MeA $^{OXTR+AI}$ or MeA $^{OXTR+VMHvl}$ caused a specific increase of consolation or aggression, respectively, but inhibition of these two populations caused the opposite result. Such results undoubtedly proved specific strong regulatory roles of the MeA $^{OXTR+AI}$ on consolation and the MeA $^{OXTR+VMHvl}$ on aggression.

Activation of the MeA $^{OXTR+AI}$ and MeA $^{OXTR+VMHvl}$ increased consolation and aggression mainly through glutamergic mechanism

According to the triple-labeled experiment of c-Fos, AAVs (2/R) tracing, and MeA OXTR under consolation or aggression in the present study (Supplementary Fig. 21), the activated MeA $^{OXTR+AI}$ neurons under consolation and activated MeA $^{OXTR+VMHvl}$ neurons under aggression distributed diffusely in both PD and PV subregions of the MeA. To better clarify the main types of the two populations, the MeA $^{OXTR+AI}$ and

MeA $^{OXTR+VMHvl}$ neurons infected with rAAV-DIO-hM4D(Gi)-mCherry were labeled by anti-vesicular glutamate transporters 2 ($VGlu2$) and anti-GABA. As shown in Fig. 9a, e and Supplementary Fig. 25, approximately 73.31% of the MeA $^{OXTR+AI}$ neurons and 78.34% of the MeA $^{OXTR+VMHvl}$ neurons were glutamergic (Fig. 9b, f). In addition, as shown in Fig. 9c, g, and Supplementary Fig. 25, only 20.81% of the MeA $^{OXTR+AI}$ neurons and 24.34% of the MeA $^{OXTR+VMHvl}$ neurons are GABAergic (Fig. 9d, h). According to these data, we could confirm that most of the MeA $^{OXTR+AI}$ and MeA $^{OXTR+VMHvl}$ neurons are glutamergic.

Then the whole-cell patch clamp recording and optogenetic stimulation were combined to verify the above-mentioned immunofluorescent results that projections from the MeA OXTR to the AI or VMHvl are excitatory (Fig. 9i). Spontaneous discharge rate induced by 473-nm LED stimulation of the AI and VMHvl neurons receiving projections from the hCHR2-MeA $^{OXTR+AI}$ or hCHR2-MeA $^{OXTR+VMHvl}$ were recorded and presented as Fig. 9j, l. 76.47% (13 cells/17 cells) of the AI neurons and 77.27% (17 cells/22 cells) of the VMHvl neurons were activated while terminals from the hCHR2-MeA $^{OXTR+AI}$ and hCHR2-MeA $^{OXTR+VMHvl}$ were photostimulated, respectively (Fig. 9k, m).

To further determine mediation of the α -amino-3-hydroxy-5-methyl-4-isoxazole-propionic acid (AMPA) receptors in activation of

the AI and VMHvl, the excitatory postsynaptic current (EPSC) was recorded while target brain slices with hCHR2 virus-infected neurons were stimulated with 473-nm LED and infused with 6-cyano-7-nitroquinoxaline-2,3-dione (CNQX, AMPA receptor antagonist) simultaneously. As representative optically-evoked EPSC (oEPSC) traces shown in Fig. 9n, p, the oEPSC amplitude of both AI and VMHvl neurons were enhanced significantly by PS. These enhanced oEPSC amplitudes could totally be abolished by infusion of CNQX (Fig. 9o, q). The AMPA receptors located in the AI and VMHvl were thus the main type of glutamate receptors through which the MeA^{OXTR+AI} and MeA^{OXTR+VMHvl} neurons exerted excitatory effects. However, whether OXTR in the MeA mediated consolation and aggression in vivo through the glutamatergic mechanism remained unknown.

To examine the mediation role of the glutamatergic system at the behavioral level, rAAV-VGlu2-DIO-mCherry/rAAV-VGlu2-DIO-hCHR2(H134R)-mCherry was injected into the MeA, and rAAV(retro)-OXTR-cre were injected to the AI or VMHvl unilaterally (Fig. 10a and Supplementary Fig. 26a). 7 days after optic fiber implantation, we

evaluate subjects' behavioral changes following stimulation of CHR2 with intermittent 473-nm LED in glutamatergic fibers at the AI or VMHvl (Fig. 10b). Figure 10c, d, f and Supplementary Fig. 26b, c showed the representative images of virus expression in the MeA and a higher firing rate during optogenetic stimulations. The specificity of VGlu2-hCHR2 and mCherry virus infection in MeA^{OXTR+AI} and MeA^{OXTR+VMHvl} were shown in Fig. 10e and Supplementary Fig. 26i. Individual channels' images for representative overlapped images of VGlu2-hCHR2 (mCherry)-MeA^{OXTR+AI(VMHvl)} cells of optogenetic experiments were shown in Supplementary Fig. 26h, i. Representative merged images of axon projections and fiber tracts were also shown in Supplementary Fig. 26j-m.

To evaluate the efficiency and specificity of rAAV-VGlu2-DIO-hCHR2 infection, 200 nl of a mixture of rAAV-VGlu2-DIO-hCHR2 and rAAV-CRE were injected into the MeA and stained with VGlu2 antibody 21 days later (Supplementary Fig. 27a-c). The result shows that 93.35% of VGlu2-hCHR2-MeA cells were labeled by the VGlu2 antibody and 76.67% of the total glutamatergic cells were infected by the VGlu2-hCHR2 virus (Supplementary Fig. 27d-f).

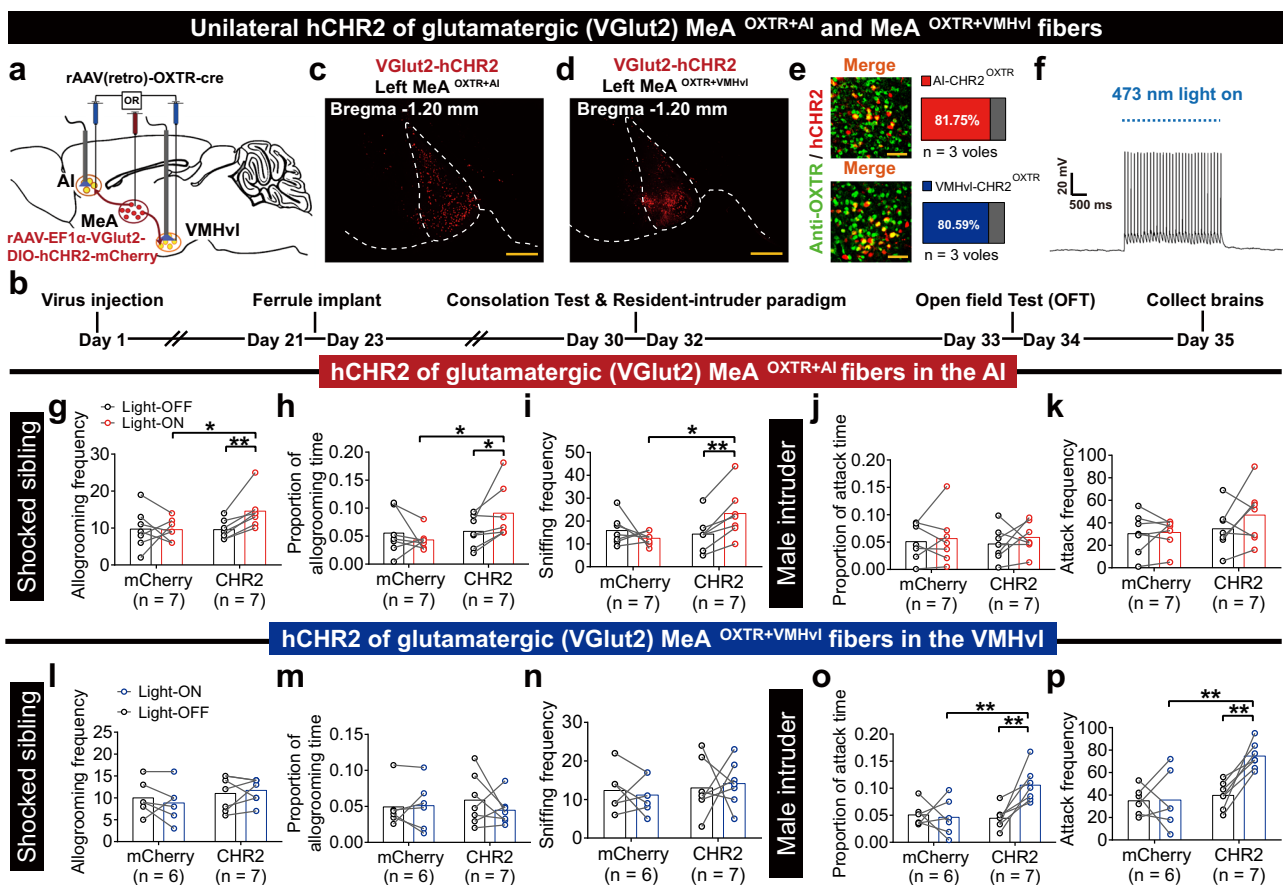


Fig. 10 | Effects of optogenetic activation of glutamatergic MeA^{OXTR+AI} and MeA^{OXTR+VMHvl} fibers on consolation and aggression. **a, b** Virus regimen (adapted from *The Mouse Brain in Stereotaxic Coordinates* by Paxinos and Franklin, **a**) and schedule (**b**) for optogenetic activation of the glutamatergic (VGlu2) fibers of the MeA^{OXTR+AI} and MeA^{OXTR+VMHvl}. **c, d** Images of VGlu2-hCHR2 expression (mCherry, red) in MeA^{OXTR+AI} and MeA^{OXTR+VMHvl}. Scale bars, 500 μ m. 7 independent repetitions with similar results in (c) and (d). **e** Representative overlapped images of VGlu2-hCHR2 somata (mCherry) and anti-OXTR (AF488, green) cells. Scale bars, 50 μ m. $n = 3$ voles/group. **f** Representative traces from electrophysiological recordings showing photoactivation of the glutamatergic MeA^{OXTR+AI} or MeA^{OXTR+VMHvl} somata. **g-k** Comparison of allogrooming and sniffing siblings, and of attacking intruders between the AI-retro VGlu2-CHR2 and VGlu2-mCherry groups. n (mCherry) = 7 voles; n (CHR2) = 7 voles. Allogrooming frequency: CHR2-Light OFF versus CHR2-Light ON, $p = 0.0041$; mCherry-Light ON versus CHR2-Light ON, $p = 0.0406$;

Allogrooming time proportion: CHR2-Light OFF versus CHR2-Light ON, $p = 0.038$; mCherry-Light ON versus CHR2-Light ON, $p = 0.032$; Sniffing frequency: CHR2-Light OFF versus CHR2-Light ON, $p = 0.006$; mCherry-Light ON versus CHR2-Light ON, $p = 0.025$. **l-p** Comparison of allogrooming and sniffing siblings, and of attacking intruders between the VMHvl-retro VGlu2-CHR2 and VGlu2-mCherry groups. n (mCherry) = 6 voles, n (CHR2) = 7 voles. Attack time proportion: CHR2-Light OFF versus CHR2-Light ON, $p = 0.003$; mCherry-Light ON versus CHR2-Light ON, $p = 0.008$; Attack frequency: CHR2-Light OFF versus CHR2-Light ON, $p = 0.002$; mCherry-Light ON versus CHR2-Light ON, $p = 0.004$. Data was analyzed by repeated measure two-way ANOVA with Sidak's multiple comparison test (**g-p**). $***p < 0.001$, $**p < 0.01$, $*p < 0.05$. Data are presented as the means \pm SEM. Statistical details are presented in the Supplementary Data 1 file. Source data are provided as a Source Data file. VGlu2 vesicular glutamate transporter 2.

Optogenetic activation of the VGlut2 terminals of the MeA^{OXTR+AI} increased allogrooming and sniffing to stressed siblings (Fig. 10g–i and Supplementary movie. 5), but did not influence aggression to male intruders (Fig. 10j, k). In contrast, optogenetic activation of the VGlut2 terminals of the MeA^{OXTR+VMHvl} increased aggression to male intruders (Fig. 10o, p and Supplementary Movie. 6), but did not affect consolation (Fig. 10l–n). In addition, 473-nm LED stimulation of glutamatergic terminals of the MeA^{OXTR+AI} or MeA^{OXTR+VMHvl} did not affect behavioral performance in OFT (Supplementary Fig. 26d–g). In addition, consolation and aggression behaviors but not performance in open field tests among subject voles were also specifically increased by photogenetic activation using virus strategy carrying CAMKII α promoters (Supplementary Figs. 28 and 29). This result was consistent with the results of photogenetic activation using a virus strategy carrying VGlut2 promoters.

Discussion

The MeA is found to be associated with consolation and aggression, but whether and how specific cell types in the MeA regulate these two types of behaviors and contribute to behavioral flexibility in different social contexts remains unclear. Using a number of different technologies to monitor and manipulate neurons in the MeA of male mandarin voles in the present study, two largely distinct subtypes of OXTR neurons in the MeA projecting to the AI or VMHvl that respond differently to stressed siblings or unfamiliar intruders and causally control consolation and aggression, respectively, were identified. These findings reveal previously unrecognized subpopulations of neurons in the MeA and circuits underlying the switch between consolation and aggression while the subjects encounter different social stimuli (Supplementary Fig. 30).

The MeA integrates chemosensory inputs from the vomeronasal network in different social interactions and generates behavioral phenotype with positive or negative valence such as anti-social (aggression) and prosocial behavior (consolation and parenting)^{21,31}, through “efferent projections to appropriate downstream regions controlling specific social behaviors”, “mediation of local multiple receptors”, “function exertion of different subregions/types of the neuronal population” and “adjustment of neuronal activity”¹⁴. Therefore, the MeA is undoubtedly a vital region to study the mechanisms of orchestrating different social sensorimotor transformations. Based on this characteristic, we hypothesized that olfactory stimuli from distressed siblings acquire the ability to activate positively valent MeA neurons that project to the AI involving prosociality^{26,32}. The odor signal from strange intruders is shown as activating negatively valent neurons that project to the VMHvl mediating aggression³³. In the present study, dual AAVs (2/R) tracing determined the existence of MeA-AI and MeA-VMHvl pathways, which were consistent with previously reported efferent regions of the MeA²³. The MeA^{AI} and MeA^{VMHvl} populations are morphologically distinct. High levels of OXTR expression were found in these two populations of neurons. Such anatomically complete separation was totally consistent with specific responses and regulations of the MeA^{OXTR+AI} and MeA^{OXTR+VMHvl} on consolation and attack, respectively, revealed by fiber photometric recording and genetic manipulation of neuronal activity.

On the one hand, increased expression of c-Fos in the MeA under consolation was observed (Supplementary Fig. 3m), which was consistent with reported positive involvement of the MeA in prosocial behavior and observational fear learning^{7,34,35}. Furthermore, it was generally accepted that OXT input from the PVN enhanced social recognition memory by inducing synaptic specific long-term depression in the olfactory bulb (AOB)-MeA pathway^{16,36}. OXT in the MeA in rodents was also found to regulate sociality³⁷, social cognition^{38,39}, interest²⁹, approach¹⁷, and preference⁴⁰. Similarly, higher levels of real-time OXT release at the MeA and more active PVN^{OXT+MeA} neurons were also detected during consoling among subject voles in the present

study (Supplementary Fig. 16). And blockade of OXTR in the MeA decreased levels of consolation (Supplementary Fig. 15). The AI, a core prosocial brain region anatomically closely connected to social decision-making network including the MeA^{23,24,26,32,41,42}, could perceive and integrate both endogenous physiological changes and sensory stimulation (e.g., olfaction) in prosocial context⁴³, then may thus control the consolation execution⁴⁴. These conclusions propose a possible hypothesis that the OXT signals acting on OXTR in the MeA regulate consolation execution by integrating processed olfactory information into the AI. In the present study, the specific increase of c-Fos expressions in the whole AI cells and the AI neurons receiving monosynaptic projections from the MeA caused by consolation were found (Supplementary Fig. 3n, Fig. 2j and Supplementary Fig. 7c). Such positive engagement of the MeA^{AI} in consolation was proved to be regulated by OXTR (Fig. 3h). Using *in vivo* fiber photometry to monitor neuronal activities of the MeA^{OXTR+AI} upon allogrooming and Opto-/Chemo-genetic manipulation of these two populations of neurons, respectively, we found that the projections from the glutamatergic OXTR neurons in the MeA to the AI could directly reflect and regulate the acute occurrence of consolation (Figs. 5–8 and 10). The contribution of AMPA receptors to consolation by activating the AI was also confirmed (Fig. 9n, o), which was consistent with its role in the basal excitatory synaptic transmission and excitatory effect in the insula cortex⁴⁵.

Noticeably, Ye Emily Wu²¹ found that activation of the medial preoptic area (MPOA)-projecting MeA^{Tachykinin1(TAC1)+GABA} populations promoted affiliative allogrooming in mice. According to the same behavioral effect in male mandarin voles by activating AI-projecting MeA^{OXTR+Glutamatergic(Glu)} populations in the present study, and the comparable fiber density of the MeA OXTR neurons to the AI and MPOA in male mandarin voles (Supplementary Fig. 1l), we proposed that the two distinct pathways may generate similar behavioral performance through totally different mechanisms. That is, the effect of the MPOA-projecting MeA^{TAC1+GABA} populations may depend on the regulatory role of the MPOA on social reward or anxiety emotion^{46–48}, but the effect of the AI-projecting MeA^{OXTR+Glu} populations may rely on the AI's executive control of consolation. These two complementary pathways both have the MeA as the core position of consolation-related neuronal networks. Such assumptions were worthy of exploring further. In addition, we also noticed that there is a combined regulatory effect of OXT signaling with secretin or estrogens in the MeA on social cognition^{49,50}, whether and how secretin or estrogens in the MeA influenced consolation by interacting with OXTR is also an interesting question.

On the other hand, c-Fos positive neurons in the MeA increased following aggression indicating recruitment of the MeA in aggression (Supplementary Fig. 3m), this result was consistent with the previous report that the MeA activity increased under aggression^{51,52}. Multiple studies also reported the necessity of the MeA in experience-dependent aggression using a lesion method⁵³. Roles of a series of neural connections including the cortico-MeA⁵⁴, anterior hypothalamus-MeA⁵², MeA-BNST⁵⁵, and the MeA-VMHvl with the MeA as an intermediate layer, in the regulation of aggression attracted the greatest attention recently^{20,56} and were also confirmed. In the present study, the specific increase of c-Fos expression under territory defensive aggression was observed in both the whole VMHvl and cells receiving monosynaptic projections from the MeA (Fig. 2n and Supplementary Fig. 3o), which was consistent with the reported increase of c-Fos after social defense⁵⁷. The involvement of the MeA^{VMHvl} in aggression was regulated by OXTR preferentially (Fig. 3h). Lin et al.³³ reported that optogenetic stimulation of the VMHvl neurons was efficient in causing nonspecific attacks to males, females, and even objects. In addition to its necessity for aggression, the VMHvl can also fit and predict diverse parameters of attack actions, and regulate acute and long-term aggression^{27,58,59}. Although the extensive role of the OXT

system on intermale aggression^{10,11}, there were few studies exploring real-time regulation of OXTR for aggression.

The increased activity of PVN^{OXTR+MeA} neurons and OXT release in the MeA during attacking were found in the present study (Supplementary Fig. 16). And OXTR antagonist infusion in the MeA reduced levels of aggression (Supplementary Fig. 15). Combined with such strong correlation between aggression and OXT system in the MeA, and reported involvement of the MeA OXT signaling⁶⁰ and MeA-VMHvl pathway in aggression, we assumed that the MeA^{OXTR} neurons could control the intensity of aggression by projecting to the VMHvl. From the results of in vivo calcium photometry and genetic manipulation, we concluded that the glutamatergic MeA^{OXTR+VMHvl} population could directly reflect and control real-time attacks (Figs. 5–8 and 10). One previous study reported that photostimulation of CHR2 to the mainly glutamatergic (85%) neurons in the PV subregion of the MeA to the VMH increased aggressive performance²⁰. These results were consistent with our finding that 78.34% of MeA^{VMHvl+OXTR} are glutamatergic (Fig. 9f). We also confirmed the excitatory inputs were mediated by AMPA receptors in the VMHvl (Fig. 9p and q), which was consistent with a previous finding that the MeA neurons to the VMHvl projections are mainly excitatory⁶¹ and CNQX could block oEPSC in the VMH(vl) receiving glutamatergic projections from the posterior and medial amygdala^{62,63}.

In the present study, subjects exhibited rapid switching and activation of the MeA^{OXTR+AI} or MeA^{OXTR+VMHvl} when facing stressed siblings or strange intruders. The specific regulation of the MeA^{OXTR+AI} and MeA^{OXTR+VMHvl} in consolation and aggressive behaviors were also established, respectively, in male mandarin voles. Therefore, although some questions need to be answered in future studies (detailed description can be found in Supplementary Discussion and Supplementary Figs. 31 and 32), our study not only clarified the MeA as a core brain region in the regulation and transformation of pro-/anti-social behavior, broadened the network for the operation of instinctive behavior at the mesoscopic level in the central nervous system (CNS), but also provided additional evidence of the potential targets for the treatments of mental disorders associated with low levels of prosocial behaviors and high levels of aggression.

Methods

Animals

Subjects used in the present study were lab-bred F2 generation of male mandarin voles (F2–F3) that were captured from Lingbao City, Henan Province, China. The voles were weaned 21 days after birth and assigned to separate polycarbonate cages (44 × 22 × 16 cm) based on their sex. The breeding room was kept under a 12 h light/12 h dark cycle at a suitable temperature (23 ± 3 °C) and humidity (55 ± 10%) and voles were free access to food and water. All male voles used in this study were 12–14 weeks old. The experimental protocols were approved by the Animal Care and Use Committee of Shaanxi Normal University and were conducted in accordance with the ethical principles of animal use and care in China.

Virus preparations

rAAV2/1-hSyn-CRE-WPRE-hGH-pA (1.18 × 10¹³ vg/mL, PT-0136), rAAV2/9-Efla-DIO-EGFP-WPRE-hGH-pA (1.14 × 10¹³ vg/mL, PT-0795), rAAV2/9-OXTR-mCherry-WPRE-pA (2.00 × 10¹² vg/mL, PT-0718), rAAV2/R-OXTR-Cre-WPRE-pA (5.00 × 10¹² vg/mL, PT-0031), rAAV2/R-OXT-Cre-WPRE-pA (6.17 × 10¹² vg/mL, PT-0263), rAAV2/9-EFla-DIO-GCaMP6m-WPRE-hGH-pA (2.64 × 10¹² vg/mL, PT-0283), rAAV2/9-EFla-DIO-taCasp3-TEVp-P2A-EGFP-WPRE-hGH-pA (2.88 × 10¹² vg/mL, PT-1230), rAAV2/9-EFla-DIO-hCHR2(H134R)-mCherry-WPRE-hGH-pA (1.00 × 10¹³ vg/mL, PT-0002), rAAV2/9-EFla-DIO-hM4D(Gi)-mCherry-WPREs (1.15 × 10¹³ vg/mL, PT-0043), rAAV2/9-EFla-DIO-mCherry-WPRE-hGH-pA (1.60 × 10¹³ vg/mL, PT-0013), rAAV2/9-CAMKIIα-DIO-mCherry-WPRE-hGH-pA (2.00 × 10¹² vg/mL, PT-1167), rAAV2/9-CAMKIIα-DIO-hCHR2(H134R)-mCherry-WPRE-

hGH-pA (2.00 × 10¹² vg/mL, PT-2059), rAAV-CAG-EGFP-WPRE-hGH-pA (2.00 × 10¹² vg/mL, PT-0305), rAAV2/9-VGlut2-DIO-mCherry-WPRE-hGH-pA (2.00 × 10¹² vg/mL, PT-3884) and rAAV2/9-VGlut2-DIO-hCHR2(H134R)-mCherry-WPRE-hGH-pA (2.00 × 10¹² vg/mL, PT-9010) and rAAV2/9-hSyn-CRE-WPREs-hGH-pA (5.35 × 10¹² vg/mL, PT-0136) were purchased from BrainVTA, China. rAAV2/R-hSyn-EGFP (5.00 × 10¹² vg/mL, BC-0020), rAAV2/R-hSyn-mCherry (5.00 × 10¹² vg/mL, BC-0023), rAAV2/9-CAG-mWGA-mCherry (2.00 × 10¹² vg/mL, BC-1170), rAAV2/9-hSyn-OXT1.0 (BC-0293) and rAAV2/9-hSyn-OXTmut (BC-0758) were purchased from BrainCase, China⁶⁴. All AAVs were aliquoted and stored at –80 °C until use.

Stereotaxic surgery

The male mandarin voles (12–14 weeks old) were anesthetized with 1.5%–3% isoflurane inhalant gas (R5-22-10, RWD, China) and fixed to a stereotaxic frame (68045, RWD, China). A median cut was made on the top of the head after being shaved and sterilized, then the connective tissue was removed. According to different experimental purposes, a 10 μL Hamilton microsyringe (7635-01, HAMILTON, Switzerland) was used to deliver different kinds of AAVs by a microsyringe pump (KDS LEGATO 130, RWD, China) at the rate of 70 nl/min. After the injection, the syringe was allowed to stay for 10 min before withdrawal in order to prevent the virus from leaking out. Then scalp was sutured. In both fiber photometry and optogenetic experiments, a fiber optical cannula (diameter: 2.5 mm, depth: 6 mm; RWD, China) was implanted into the site 0.15 mm above the target regions 3 weeks after virus injection except 1 week after injections of rAAV2/9-hSyn-OT1.0 or rAAV2/9-hSyn-OTmut. In order to block OXTR in the MeA using pharmacological methods, cannula guide tubes (OD: 0.41 mm; ID: 0.20 mm) were implanted into the bilateral MeA with a 1.0 mm separation. The injection coordinates were as follows: PVN (AP: –0.45, ML: ±0.4, DV: –5.40); MeA (AP: –1.18, ML: ±2.4, DV: –5.45); AI (AP: +0.95, ML: ±3.94, DV: –3.97); VMHvl (AP: –1.22, ML: ±0.66, DV: –5.76).

c-Fos immunostaining of the MeA, AI, and VMHvl

To investigate whether the MeA and AI during consolation and the MeA and VMHvl during aggression show high neuronal activity, subjects were divided into four groups randomly: voles whose siblings were treated to separated only (the Separation group), group-housed voles (the CON group), voles exposed to stressed siblings under consolation test (the Consolation group) and the voles displaying attack to male intruder under resident-intruder paradigm (the Aggression group). Brains were collected 90 min after treatments. Then the ×10 fluorescent images of c-Fos positive cells (stained by Cy3) in the both posterior dorsal (PD) and posterior ventral (PV) subregions of the MeA, AI, and VMHvl under the above-mentioned four treatments were quantified by image J (V1.8.0, National Institutes of Health, USA). Individual means were obtained from 5 sections and 40 μm per section, the AI ranged from bregma +1.20 mm to +0.70 mm; the VMHvl ranged from bregma –1.10 mm to –1.40 mm; the MeA ranged from bregma –1.05 mm to –1.35 mm (for counting Fos positive cells in the 0.09 mm² area of the PD and PV, *n* = 7 voles in Separation group, *n* = 6 voles in CON group, *n* = 5 voles in Consolation group, *n* = 6 voles in Aggression group; for counting Fos positive cells in AI, *n* = 6 voles in Separation group, *n* = 6 voles in CON group, *n* = 6 voles in Consolation group, *n* = 5 voles in Aggression group; for counting Fos positive cells in VMHvl, *n* = 7 voles in Separation group, *n* = 6 voles in CON group, *n* = 7 voles in Consolation group, *n* = 5 voles in Aggression group).

Dual-retrograde rAAVs (2/R) tracing

To confirm the existence of MeA-AI and MeA-VMHvl pathways and the morphological distribution of the MeA^{AI} and MeA^{VMHvl}, 250 nl of rAAV2/R-hSyn-EGFP and 150 nl of rAAV2/R-hSyn-mCherry was injected into the AI and VMHvl, respectively. Brains were collected 30 days after the virus injection. Then the ×10 images showing different virus-positive

and merged cells at the MeA were collected and quantified: the selected boxed areas ($300\ \mu\text{m} \times 300\ \mu\text{m}$) in the posterior ventral (PV) and posterior dorsal (PD) parts of the MeA were both used to count numbers of the $\text{MeA}^{\text{AI(EGFP)}}$, $\text{MeA}^{\text{VMHvl(mCherry)}}$ and $\text{MeA}^{\text{AI(EGFP)+VMHvl(mCherry)}}$ neurons (5 sections per brain: bregma -0.85 , -1.04 , -1.20 , -1.36 and -1.52 mm, $40\ \mu\text{m}$ per section). Data from 5 voles with correct positions of virus injection were used for analysis.

c-Fos immunostaining of the AI and VMHvl neurons receiving projections from the MeA

For the measurement of activities of AI or VMHvl neurons receiving projections from the MeA under different behaviors, co-labeling of neurons infected with monosynaptic anterograde rAAV (2/1) and c-Fos positive neurons was conducted. Briefly, 150 nl of rAAV (2/1)-hSyn-CRE was injected into the MeA, 80 nl or 120 nl of rAAV (2/9)-Efla-DIO-EGFP was injected into the VMHvl or AI, respectively. 21 days after injection, the subject voles were exposed to the consolation test (Consolation group) or resident-intruder paradigm (Aggression group) to induce allogrooming or attack. Separation voles (Separation group) whose siblings were housed separately only (without footshock). Group-housed voles (CON group) were treated with 10-min interaction with normal siblings. Brains were collected 90 min after treatments. The $\times 20$ and $\times 10$ images including the AI and VMHvl were obtained, then the representative boxed areas ($200\ \mu\text{m} \times 200\ \mu\text{m}$) were selected to count $\text{AI}^{\text{c-Fos(Cy3)+MeA(EGFP)}}$ and $\text{VMHvl}^{\text{c-Fos(Cy3)+MeA(EGFP)}}$ cells (5 representative sections per brain, $40\ \mu\text{m}$ per section). voles with correct positions of virus injection and expression were used for data analysis ($n = 3$ voles for counting $\text{AI}^{\text{c-Fos+MeA}}$ neurons in Separation group, $n = 3$ voles for counting $\text{AI}^{\text{c-Fos+MeA}}$ neurons in CON group, $n = 4$ voles for counting $\text{AI}^{\text{c-Fos+MeA}}$ neurons in Consolation group, $n = 5$ voles for counting $\text{AI}^{\text{c-Fos+MeA}}$ neurons in Aggression group; $n = 3$ voles for counting $\text{VMHvl}^{\text{c-Fos+MeA}}$ neurons in Separation group, $n = 4$ voles for counting $\text{VMHvl}^{\text{c-Fos+MeA}}$ neurons in CON group, $n = 5$ voles for counting $\text{VMHvl}^{\text{c-Fos+MeA}}$ neurons in Aggression group, $n = 5$ voles for counting $\text{VMHvl}^{\text{c-Fos+MeA}}$ neurons in Consolation group).

The EGFP-marked AI (VMHvl) neurons receiving projections from the MeA could project to downstream brain regions (second-grade terminals), which thus could be also marked with EGFP. By screening co-labeled regions with the second-grade terminals (EGFP) and c-Fos positive neurons (stained by Cy3) in the whole brains ($40\ \mu\text{m}$ per section), the efferent regions of the AI^{MeA} and $\text{VMHvl}^{\text{MeA}}$, which are strongly correlated with consolation and aggression, respectively, were further expanded. 3 voles were used in each for screening co-labeling of efferent regions of the AI^{MeA} ($\text{VMHvl}^{\text{MeA}}$) and c-Fos under consolation (aggression).

To further validate the AAV1 (cre-DIO system) for anterograde transsynaptic labeling, 250 nl of rAAV2/9-CAG-mWGA-mCherry was injected into the MeA. The Separation, CON, Consolation, and Aggression treatments were introduced 21 days after virus injection. Brains were collected 90 min after treatments. The $\times 20$ images including the AI and VMHvl were obtained, and then the representative boxed areas ($300\ \mu\text{m} \times 300\ \mu\text{m}$) were selected to count $\text{AI}^{\text{c-Fos(AF488)+MeA(mCherry)}}$ and $\text{VMHvl}^{\text{c-Fos(AF488)+MeA(mCherry)}}$ cells (5 representative sections per brain, $40\ \mu\text{m}$ per section). Data from voles with correct positions of virus injection and expression were included for data analysis ($n = 3$ voles for co-labeling of the AI^{MeA} and $\text{AI}^{\text{c-Fos}}$, and $\text{VMHvl}^{\text{MeA}}$ and $\text{VMHvl}^{\text{c-Fos}}$ in Separation group; $n = 3$ voles for co-labeling of the AI^{MeA} and $\text{AI}^{\text{c-Fos}}$, and $\text{VMHvl}^{\text{MeA}}$ and $\text{VMHvl}^{\text{c-Fos}}$ in CON group; $n = 3$ voles for co-labeling of AI^{MeA} and $\text{AI}^{\text{c-Fos}}$, and $\text{VMHvl}^{\text{MeA}}$ and $\text{VMHvl}^{\text{c-Fos}}$ in Consolation group; $n = 3$ voles for co-labeling of AI^{MeA} and $\text{AI}^{\text{c-Fos}}$, and $\text{VMHvl}^{\text{MeA}}$ and $\text{VMHvl}^{\text{c-Fos}}$ in Aggression group).

It should be noticed that the AAV1 (cre-DIO system) and mWGA (CAG system) viral strategies are not strictly anterograde tracers. They may produce less retrograde traces. To eliminate the possible false positive results caused by the limitations of the virus strategy itself, the

rAAV2/9-CAG-EGFP-WPRE-hGh-pA was injected into the left AI/VMHvl to determine whether these two brain regions send projections to MeA. The $\times 10$ Z-stack ($30\ \mu\text{m}$) images of axon projection of AI/VMHvl cells to the MeA were observed and collected by high-resolution laser confocal microscope (S1800769, TCSSP8, Leica, Germany).

Evaluation of efficiency and specificity of OXTR antibody

For examining the effectiveness of the OXTR antibody, the RNA-Protein Co-Detection Ancillary Kit (Advanced Cell Diagnostics 323180) was used according to the manufacturer's instructions. Briefly, the $12\text{-}\mu\text{m}$ brain sections including the MeA were conducted with tissue block and target retrieval and then incubated in OXTR antibody at $4\ ^\circ\text{C}$ over two nights. Sections were then incubated with fluorophore-conjugated secondary antibodies (anti-rabbit goat conjugated with AF-488, AB_2338000, JacksonImmuno, USA, 1: 400) after hybridization with amplifiers. Sections were then counterstained with DAPI (RNAscope® Multiplex Fluorescent Reagent Kit v2, Advanced Cell Diagnostics 323100) for 30 s at $26\ ^\circ\text{C}$. The glass slides were fixed with an antifade solution and $\times 40$ images were acquired under a high-resolution laser confocal microscope (S1800769, TCSSP8, Leica, Germany). Then the percentage of co-labeling neurons in antibody-positive neurons and in RNAscope-positive neurons were analyzed by Image J software. Data from 5 voles (5 sections per brain: bregma -1.04 , -1.12 , -1.20 , -1.28 , and -1.36 mm) were used for analysis.

Triple-labeling of dual-retrograde AAVs (2/R) tracing and anti-OXTR

For verifying MeA OXTR neurons projecting to VMHvl or AI, and investigating the morphological distribution of the $\text{MeA}^{\text{OXTR+AI}}$ and $\text{MeA}^{\text{OXTR+VMHvl}}$, 250 nl of rAAV2/R-hSyn-EGFP and 150 nl of rAAV2/R-hSyn-mCherry was injected into the AI and VMHvl, respectively. Brains were collected 30 days after the virus injection. Brain sections were labeled by fluorescently conjugated secondary antibodies (AF647, magenta) of the OXTR antibody. $\times 10$ images including the MeA were acquired, and then the selected boxed areas ($300\ \mu\text{m} \times 300\ \mu\text{m}$) of the PV and PD parts were both used to count the $\text{MeA}^{\text{OXTR(AF647)+AI(EGFP)}}$, $\text{MeA}^{\text{OXTR(AF647)+VMHvl(mCherry)}}$ and $\text{MeA}^{\text{OXTR(AF647)+AI(EGFP)+VMHvl(mCherry)}}$ neurons (5 sections per brain: bregma -0.85 , -1.04 , -1.20 , -1.36 and -1.52 mm, $40\ \mu\text{m}$ per section). To further test the preference of the MeA^{AI} and $\text{MeA}^{\text{VMHvl}}$ regulated by OXTR, the proportion of $\text{MeA}^{\text{OXTR+AI}}/\text{MeA}^{\text{AI}}$, $\text{MeA}^{\text{OXTR+VMHvl}}/\text{MeA}^{\text{VMHvl}}$ were also calculated and compared with the proportion of $\text{MeA}^{\text{OXTR}}/\text{DAPI}$. 4 voles with correct positions of injection were used for data analysis.

Quantification of the density of OXTR-ir fibers

For evaluating OXTR fibers density between the AI, MPOA, VMHvl, and BNST, 300 nl of rAAV2/9-OXTR-mCherry was injected in the MeA after verification of transfection efficiency of the virus by OXTR antibody (OXTR positive cells were counted in the selected $300\ \mu\text{m} \times 300\ \mu\text{m}$ areas, 5 sections per brain: bregma -0.85 , -1.04 , -1.20 , -1.36 , and -1.52 mm, $40\ \mu\text{m}$ per section, $n = 3$ voles). Brains were collected 30 days after the virus injection. Then $\times 20$ Z-stack images for $30\ \mu\text{m}$ including the four regions were acquired (4 sections per brain, $35\ \mu\text{m}$ per section), and then the selected boxed areas ($300\ \mu\text{m} \times 300\ \mu\text{m}$) were used to export the integrated optical density (IOD). Data from 4 voles with correct positions of injection and virus expression were used for analysis.

c-Fos immunostaining of two populations of neurons

For measurement of activities of MeA OXTR neurons projecting to the VMHvl or AI, co-labeling of c-Fos (Cy3), AAV (2/R)-EGFP, and anti-OXTR (AF405, magenta) caused by specific behavior was used. 250 nl (150 nl) of rAAV2/R-hSyn-EGFP was injected into the AI (VMHvl). 30 days after virus injection, the voles were introduced to the consolation test (Consolation group) or resident-intruder paradigm (Aggression

group). Separation voles (Separation group) whose siblings were housed separately only (without footshock), group-housed voles (Con group) interacted with normal siblings for 10 min. Brains were collected 90 min after treatments. In order to co-staining OXTR and c-Fos antibodies from the same host (rabbit), the 4-color staining kit (Absin, abs50028, China) was used in accordance with the manufacturer's instructions⁶⁵. The $\times 10$ images including the MeA were collected, and the selected boxed areas ($300 \mu\text{m} \times 300 \mu\text{m}$) of the PV and PD parts were both used to count the MeA^{OXTR(AF405)+AI(EGFP)+c-Fos(Cy3)} or MeA^{OXTR(AF405)+VMHvl(EGFP)+c-Fos(Cy3)} cells (5 sections per brain: bregma -0.85 , -1.04 , -1.20 , -1.36 and -1.52 mm, $40 \mu\text{m}$ per section). voles with correct positions of virus injection and expression were used for data analysis ($n = 4$ voles for triple labeling of MeA^{OXTR+AI+c-Fos} in the Separation group, $n = 4$ voles for triple labeling of MeA^{OXTR+AI+c-Fos} in the Con group, $n = 3$ voles for triple labeling of MeA^{OXTR+AI+c-Fos} in the Consolation group; $n = 4$ voles for triple labeling of MeA^{OXTR+VMHvl+c-Fos} in the Separation group, $n = 3$ voles for triple labeling of MeA^{OXTR+VMHvl+c-Fos} in the Con group, $n = 3$ voles for triple labeling of MeA^{OXTR+VMHvl+c-Fos} in the Aggression group).

VGlut2/GABA immunostaining of two populations of neurons

In this experiment, neurons co-labeling of VGlut2/GABA antibody and hM4D(Gi) were quantified. $\times 20$ (for staining VGlut2, AF488) and $\times 10$ (for staining GABA, AF488) images including the MeA were acquired, and boxed areas ($200 \mu\text{m} \times 200 \mu\text{m}$) were selected to quantify the percentage (%) of glutamatergic and GABAergic neurons in the MeA^{VMHvl(mCherry)+OXTR} or MeA^{AI+OXTR(mCherry)} neurons (6 representative sections per brain, $40 \mu\text{m}$ per section). 3 voles were for calculating the percentage of VGlut2 positive OXTR neurons in both MeA^{VMHvl+OXTR} or MeA^{AI+OXTR}; 6 voles were for calculating the percentage of GABA positive OXTR neurons in the MeA^{AI+OXTR}; 5 voles were for calculating the percentage of GABA positive OXTR neurons in the MeA^{VMHvl+OXTR}.

Assessment of the virally expressed efficiency

In this experiment, $\times 10$ images including the MeA or PVN were collected and selected boxed areas ($200 \mu\text{m} \times 200 \mu\text{m}$) were used to quantify the co-labeled percentage (%) of the cells infected with rAAVs (including CHR2 (mCherry), CAMKII α -CHR2 (mCherry), VGlut2-CHR2 (mCherry), GCaMP (EGFP), hM4D(Gi, mCherry), OXTR-mCherry in the anti-OXTR cells (5 sections per brain: bregma -1.04 , -1.12 , -1.20 , -1.28 and -1.36 mm, $40 \mu\text{m}$ per section) in the anti-OXT cells (5 sections per brain: -0.37 , -0.41 , -0.45 , -0.49 , -0.53 mm, $40 \mu\text{m}$ per section). $n = 3$ vole in each group.

For confirming cell death caused by Caspase3 and success of expression after injection of rAAV-Caspase3 virus, $\times 10$ images including the MeA were collected and selected boxed areas ($300 \mu\text{m} \times 300 \mu\text{m}$) were used to comparing numbers of OXTR positive cells between the Caspase3 and EGFP groups ($n = 4$ voles in the AI-retro EGFP group, $n = 3$ voles in the AI-retro Casp3 group; $n = 4$ voles in the VMHvl-retro EGFP group, $n = 3$ voles in the VMHvl-retro Casp3 group).

For validating the infection of VGlut2-DIO-hCHR2 to make sure that it is indeed to infect glutamatergic neurons specifically, the 100 nl of rAAV2/9-VGlut2-DIO-hCHR2-mCherry and 100 nl of rAAV2/9-hSyn-CRE-WPREs-hGH were mixed and then injected into the MeA. After 21 days of virus infection, the brain slices were stained with VGlut2 and GABA antibodies. Selected boxed areas ($200 \mu\text{m} \times 200 \mu\text{m}$) of the $\times 20$ images including the MeA were used to quantify the percentage (%) of cells infected with rAAV-VGlut2-hCHR2 in the total anti-VGlut2 positive cells or the anti-GABA positive cells (4 sections of typical MeA position per brain, $40 \mu\text{m}$ per section). 3 voles' brains were used for quantification analysis.

Apoptosis

For revealing the necessity of the MeA^{OXTR+VMHvl} and MeA^{OXTR+AI} populations in aggression and consolation, respectively, the apoptosis

(taCasp3) strategy was used to ablate these neurons. 150 nl of rAAV-EF1 α -DIO-taCasp3-TEVp-P2A-EGFP was injected into the MeA, and 75 nl (100 nl) of rAAV2/R-OXTR-Cre was injected into the VMHvl (AI) bilaterally. Control voles were injected with 150 nl rAAV-EF1 α -DIO-EGFP into the MeA and 75 nl (100 nl) of rAAV2/R-OXTR-Cre was injected into the VMHvl (AI) bilaterally.

30 days after virus injection, voles were subjected to the consolation test, followed by the resident-intruder paradigm. Each test lasted for 10 min with at least 5 min intervals. voles with correct bilateral injection and expression of taCasp3-TEVp-P2A-EGFP or EGFP in the MeA were used for data analysis ($n = 7$ for MeA^{OXTR+AI(taCasp3)} apoptosis, $n = 7$ for MeA^{OXTR+AI(EGFP)} as control; $n = 7$ for MeA^{OXTR+VMHvl(taCasp3)} apoptosis, $n = 7$ for MeA^{OXTR+VMHvl(EGFP)} as control).

Pharmacology

To explore whether OXTR signaling in the MeA plays a causal role in regulating consolation or aggression, the pharmacological method was applied to block the OXTR function. 10-day recovery after implantation of the bilateral cannula to the MeA, subject voles were anesthetized with isoflurane and given a bilateral injection of vehicle (saline, 200 nl/side). Then their behavioral performance in the consolation test and resident-intruder paradigm were recorded 15 min after saline infusion (recovery from anesthesia). Each test lasted for 10 min with 5 min intervals. After 2-day interval, subjects were subjected to the two types of testing 15 min after injection of a vehicle containing an OXTR antagonist (OXTR-A, [(D CH2) 5I, Tyr (Me) 2, Thr4, Orn8, des-Gly-NH29]-Vasotocin trifluoroacetate salt) (0.5 ng/200 nl per side). The dose of OXTR-A administration was chosen based on previous studies with OXTR-A^{6,38,39}. Subject voles with correct bilateral cannula placement were used for analysis ($n = 8$ voles in each group).

Fiber photometry

For recording fluorescent dynamics of the MeA^{OXTR sensor} using fiber photometry upon consoling, attacking, and investing new objects, 200 nl of rAAV2/9-hSyn-OXT1.0 was injected into the MeA. Control voles were injected with 200 nl rAAV2/9-hSyn-OXTmut into the MeA unilaterally. One week after the virus injection, a fiber optical cannula (diameter: 2.5 mm, depth: 6 mm) was implanted 0.15 mm above the left MeA and fixed by dental cement (19-7220, HWAYON BIOTECH, China). The changes in fluorescent signal were detected one week after cannula implantation. Data from voles with correct sites of virus injection and fiber implantation with correct expression of OXT sensor and OXT mut were used for analysis ($n = 6$ voles for recording the signal of MeA^{OXTR sensor}, $n = 5$ voles for recording the signal of MeA^{OXTR mut (EGFP)} as control).

For recording of the PVN^{OXTR+MeA} neuronal activities using fiber photometry upon consoling, attacking, and investing new object, 200 nl of rAAV-EF1 α -DIO-GCaMP6m-EGFP was injected into the PVN, and 150 nl of rAAV2/R-OXT-Cre-WPRE-pA was injected into the MeA. Control voles were injected with 200 nl of rAAV-EF1 α -DIO-EGFP into the PVN and 150 nl of rAAV2/R-OXT-Cre-WPRE-pA into the MeA unilaterally. 3 weeks after the virus injection, a fiber optical cannula was implanted 0.15 mm above the left PVN. The changes in calcium signal were detected 1 week after cannula implantation. Data from voles with correct expression of GCaMP6m-EGFP and EGFP were used for analysis ($n = 6$ voles for recording the signal of PVN^{OXTR+MeA(GCaMP)}, $n = 5$ voles for recording the fluorescent signal of PVN^{OXTR+MeA(EGFP)} as control).

For fiber photometry recording of the MeA^{OXTR+VMHvl} and MeA^{OXTR+AI} populations during consolation, resident-intruder and new object recognition tests, 150 nl of rAAV-EF1 α -DIO-GCaMP6m-EGFP was injected into the MeA, and 75 nl (100 nl) of rAAV2/R-OXTR-Cre was injected into the VMHvl (AI) unilaterally. Control voles were injected with 150 nl of rAAV-EF1 α -DIO-EGFP into the MeA and 75 nl (100 nl) of rAAV2/R-OXTR-Cre was injected into the VMHvl (AI) unilaterally. 3 weeks after

the virus injection, a fiber optical cannula was implanted 0.15 mm above the left MeA. The changes in calcium signal were detected one week after cannula implantation. voles with correct unilateral expression of DIO-GCaMP6m-EGFP and DIO-EGFP were used for data analysis ($n = 6$ voles for recording the calcium signal of MeA^{OxTR+Al(GCaMP6m)}, $n = 9$ voles for recording the fluorescent signal of MeA^{OxTR+Al(EGFP)} as control; $n = 7$ voles for recording the calcium signal of MeA^{OxTR+VMHvl(GCaMP6m)}, $n = 8$ voles for recording the fluorescent signal of MeA^{OxTR+VMHvl(EGFP)} as control).

Fiber photometry was implemented as previously described^{28,66}. In brief, the emission light from modulated blue 473-nm LED was reflected with a dichroic mirror, and then delivered to the brain by an optical objective lens coupled to an optical commutator, which excited the OXT sensor in the MeA, and GCaMP6m located in the PVN and MeA. The light was passed through another band pass filter, into a high-sensitivity CMOS detector (DCC3240M, Thorlabs Inc, USA), and finally visualized by TDMSViewer (a Labview program, ThinkerTech Nanjing Bioscience, China). On the testing day, the voles were anesthetized with 1.5%–3% isoflurane gas and then connected to a multi-mode optic fiber patch cord (NA: 0.37, OD: 200 μ m; ThinkerTech Nanjing Bioscience, China), and its other end was connected to a fiber photometry apparatus (QAXK-FPS-MC-LED for recording signals of the MeA^{OxTR+VMHvl} and MeA^{OxTR+Al} populations, QAXK-FPS-TC-MC-LED for recording signals of the MeA^{OxT sensor} and PVN^{OxT+MeA}, ThinkerTech Nanjing Bioscience, China). After 25-min habituation, the voles were subjected to the consolation test, the resident-intruder paradigm, fluorescence changes of the MeA^{OxT sensor}, PVN^{OxT+MeA}, MeA^{OxTR+Al}, and MeA^{OxTR+VMHvl} populations upon the social and non-social behaviors were all recorded. Finally, voles were exposed to the same cage alone, changes in fluorescence signals were also recorded while voles were sniffing objects (little Rubik's Cube). The interval between tests was at least 5 min. If a specific behavior occurred no more than four times within 25 min, the recording was replicated on the following day.

All data of photometric signals in this study were analyzed by Multi Fiber Photometry (a custom-written MATLAB software, ThinkerTech Nanjing Bioscience, China), which is available at MATLAB 2019a⁶⁷. Briefly, the waveform indicating changes in the calcium signal would float relative to the baseline at the moment when the specific behavior occurs. The whole data were divided into averaged fluorescence signals of a period before the stimulation (F₀) and behavioral events-related signal F . F_0 represents the baseline fluorescence signal averaged over a 10 s-long control time window. The $(F - F_0)/F_0$ (delta F/F) was to characterize event-related fluorescence intensity of all trials of a particular behavior. The whole data was first segmented according to the behavioral events. Then the time window was determined based on the duration of a behavior bout. In this study, pre-phases were totally set as 2 s; the post-phases of sniffing behaviors (including to siblings, intruders, and objects) were set as 2 s; the post-phases of both allogrooming and attack were set as 3 s according to durations of these behaviors scored and analyzed by J watcher software (<https://www.jwatcher.ucla.edu/>, Dan Blumstein's Lab & the late Christopher Evans' lab, Sydney). Finally, we calculated the average value of calcium signals in both pre-(2 s) and post-phases (2 s or 3 s), and the AUC per second was the key indicator to compare calcium signals before and after the specific event or revealed the changes in calcium signal after the occurrence of different behaviors.

Optogenetic activation

For verifying the immediate effects of activating the MeA^{OxTR+Al} and MeA^{OxTR+VMHvl} somata and fibers on aggression and consolation, 150 nl of rAAV-EF1 α -DIO-hCHR2(H134R)-mCherry was injected into the MeA, and 75 nl (100 nl) of rAAV2/R-OXTR-Cre was injected into the VMHvl (AI) unilaterally. Control voles were injected with 150 nl rAAV-EF1 α -DIO-

mCherry into MeA and 75 nl (100 nl) of rAAV2/R-OXTR-Cre was injected into the VMHvl (AI) unilaterally. 3 weeks after virus injection, a fiber optical cannula (diameter: 2.5 mm, depth: 6 mm) was implanted 0.15 mm above the position of virus injection in the MeA or the AI (VMHvl) to activate somata and fibers, respectively. The optogenetic stimulation was conducted one week after cannula implantation. voles with correct unilateral injection and expression of DIO-hCHR2-mCherry and DIO-mCherry were used for data analysis ($n = 9$ voles for optogenetic activation of MeA^{OxTR+Al(hCHR2)} somata, $n = 6$ voles for MeA^{OxTR+Al(mCherry)} as control; $n = 8$ voles for optogenetic activation of MeA^{OxTR+VMHvl(hCHR2)} somata, $n = 6$ voles for MeA^{OxTR+VMHvl(mCherry)} as control. $n = 7$ voles for optogenetic activation of MeA^{OxTR+Al(hCHR2)} fibers, $n = 6$ voles for MeA^{OxTR+Al(mCherry)} as control; $n = 7$ voles for optogenetic activation of MeA^{OxTR+VMHvl(hCHR2)} fibers, $n = 6$ voles for MeA^{OxTR+VMHvl(mCherry)} as control).

For confirming the activation effects of the MeA^{OxTR+Al} and MeA^{OxTR+VMHvl} on consolation and aggression were mainly through glutaminergic mechanism, 200 nl of rAAV2/9-CAMKII α (VGlut2)-DIO-hCHR2(H134R)-mCherry was injected into the MeA, and 100 nl (150 nl) of rAAV2/R-OXTR-Cre was injected into the VMHvl (AI) unilaterally. Control voles were injected with 200 nl rAAV2/9-CAMKII α (VGlut2)-DIO-mCherry into MeA and 100 nl (150 nl) of rAAV2/R-OXTR-Cre was injected into the VMHvl (AI) unilaterally. 3 weeks after the virus injection, a fiber optical cannula was implanted in the AI (VMHvl). The optogenetic stimulation was conducted 1 week after cannula implantation. Data from voles with correct unilateral virus injection, fiber implantation, and expression of CAMKII α (VGlut2)-DIO-hCHR2-mCherry and CAMKII α (VGlut2)-DIO-mCherry were used for data analysis ($n = 6$ voles for optogenetic activation of MeA^{OxTR+Al(CAMKII α -hCHR2)} fibers, $n = 6$ voles for MeA^{OxTR+Al(CAMKII α -mCherry)} as control; $n = 6$ voles for optogenetic activation of MeA^{OxTR+VMHvl(CAMKII α -hCHR2)} fibers, $n = 6$ voles for MeA^{OxTR+VMHvl(CAMKII α -mCherry)} as control; $n = 7$ voles for optogenetic activation of MeA^{OxTR+Al(VGlut2-mCherry)} fibers, $n = 7$ voles for MeA^{OxTR+Al(VGlut2-hCHR2)} as control; $n = 7$ voles for optogenetic activation of MeA^{OxTR+VMHvl(VGlut2-hCHR2)} fibers, $n = 6$ voles for MeA^{OxTR+VMHvl(VGlut2-mCherry)} as control).

Optogenetic equipment and settings were used as in a previous study^{28,66}. Ferrules were connected (by patch cords) to a 473-nm laser diode of the optogenetic smart light source (Aurora 300, NEWDOON INC, China) through an FC/PC adaptor and a fiber optic rotary joint. The output parameters were 10-ms pulses, 20 Hz, 8-s on and 2-s off cycle, 5 mW for stimulating somata, and 10 mW for stimulating (glutamatergic) axon fibers. Behaviors in the 10-min consolation test, 10-min resident-intruder paradigm, and 5-min OFT were recorded and scored while photostimulation (PS) was ON or OFF.

Pharmacogenetic inhibition

For pharmacogenetic inhibition of the MeA^{OxTR+VMHvl} and MeA^{OxTR+Al} neuron populations, 150 nl of rAAV2/9-EF1 α -DIO-hM4D(Gi)-mCherry was injected into the MeA, and 75 nl (100 nl) of rAAV2/R-OXTR-Cre was injected into the VMHvl (AI) bilaterally. Control voles were injected with 150 nl rAAV-EF1 α -DIO-mCherry into the MeA and 75 nl (100 nl) of rAAV2/R-OXTR-Cre was injected into the VMHvl (AI) bilaterally. voles with correct bilateral virus injection and expression of DIO-Gi-mCherry and DIO-mCherry in the MeA were used for data analysis ($n = 7$ voles for inhibiting MeA^{OxTR+Al(Gi)}, $n = 7$ voles for MeA^{OxTR+Al(mCherry)} as control; $n = 5$ voles for inhibiting MeA^{OxTR+VMHvl(Gi)}, $n = 7$ voles for MeA^{OxTR+VMHvl(mCherry)} as control).

Three weeks after virus injection, all behavioral tests were conducted among subjects 30 min after intraperitoneal injection of saline or CNO (clozapine N-oxide, 1 mg/kg, CNO-02, BrainVTA, China). During each test, the subject vole first encountered a stressed sibling for 10 min, and then the sibling was removed for 5 min, the subject vole encountered a non-aggressive male stranger vole for another 10 min.

Subject vole also freely moved on the open field (OFT) for 5 min after injection of saline or CNO.

Behavioral test

Digital videos of the consolation test and resident-intruder paradigm were scored by raters who were blinded to the experimental groups and treatments using J Watcher software. Behaviors in the Open-field test were automatically scored and analyzed by a Smart video tracking system (V 3.0.06, Panlab Harvard Apparatus®, Spain). All behavioral studies were conducted in dim and quiet environments between 8:30 am and 5:30 pm. After each test, the voles were returned to their home cages. For fiber photometry and optogenetic experiments, all voles were allowed to habituate to patch cords for 30 min (once per day, 3 days) before testing days, and allowed to acclimate the status of the connection to optogenetic equipment for 20 min before the test started. All definitions of main behavioral indicators were presented in Supplementary Table 1.

Consolation test

The consolation test was used to evaluate subject voles' prosocial level⁶. Briefly, male subjects cohabited with a same-sex sibling after weaning to form and maintain a close bond with each other. On the testing day, the subject voles were left alone in home cages. At the same period, the subjects' siblings were subjected to 10 repetitions of moderate electronic foot shock (3 s, 0.8 mA, 2-min interval between each shock) in a Shuttle Box (JLBehv-STM-4, Shanghai Jiliang Software Technology Co. Limited, China). Then the subjects were exposed to the foot-shocked siblings after the separation in the home cages. The behaviors of subject voles were recorded by HD camera for 10 min, and analyzed by J Watcher. Allogrooming and sniffing siblings were recorded and quantified. For optogenetic experiments, the subject was habituated to patch cords during the period when their siblings received foot shocks.

Resident-intruder paradigm

The resident-intruder paradigm was performed as described in the previous study²⁰ to assess individual's levels of territorial defensive aggression. On the testing day, subject voles were allowed to acclimate for 10 min in home cages alone after the consolation test as residents. Then a group-housed non-aggressive male stranger was induced to subjects' home cages as intruders, and the two voles were allowed to interact freely for 10 min. The test with rare or excessive aggression (causing overmuch damage to intruders) would be immediately stopped and excluded from the final analysis. All subject voles' behaviors were recorded by HD camera and scored and analyzed by raters using J Watcher. Attack and sniffing intruders were recorded and quantified. For optogenetic experiments, a fiber optic rotary joint was used to avoid optical fibers detached from the voles' heads because of the frequent pulling of patch cords during the attack.

Open-field test

The open field test (OFT) was aimed to assess the anxiety level and locomotion of subjects²⁸. Voles were placed in the square open field (50 cm × 50 cm) for 5 min free exploration. Traveled distance, time spent in the center, entry frequency in the center, and max speed were automatically recorded and quantified using Smart 3.0.

For evaluating the relieving effect of consolation on stressed emotion, stressed siblings were allowed to freely move on the open field for 25 min, and time spent in the four corners was recorded by smart 3.0²¹. Then their blood was sampled for the detection of cortisol levels as follows.

Blood sampling and cortisol (CORT) assays

For confirming the buffering effect of consolation from subjects on foot-shocked siblings' stressed emotion, sibling voles (control,

shocked and reunion, and shocked only) were deeply anesthetized with 1.5%–3% isoflurane gas, and then blood was collected from a small incision on the left atrium immediately after stress-relieving evaluation (OFT)⁶⁸. Collected blood was placed at room temperature for 20 min until coagulation, then was under centrifugation at 1500 g for 15 min to get serum, which could be stored at –80 °C refrigerator until further analysis. Serum concentrations of CORT were determined by a commercially available Mouse ELISA Kit (D721183-0096, Sangon Biotech, China) according to the manufacturer's instructions. All samples were performed in duplicate. The intra and inter-assay coefficients of variation were 8.5% and 10%, respectively.

Whole-cell patch clamp electrophysiology

The male voles were deeply anesthetized with 1.5%–3% isoflurane gas after a 3-week recovery, and the brains were quickly dissected out. 300- μ m coronal slices containing the MeA (AI and VMHvl) were prepared in a vessel full of artificial cerebrospinal fluid (ACSF) (32–34 °C) using a Leica VT1200s vibratome. The concentration of each component of ACSF was as follows: 125 mM NaCl, 2.5 mM KCl, 25 mM glucose, 25 mM NaHCO₃, 1.25 mM NaH₂PO₄, 2 mM CaCl₂, and 1 mM MgCl₂, gassed with 5% CO₂/95% O₂⁶². Then, the slices were incubated in oxygenated (5% CO₂/95% O₂) ACSF at 32–34 °C and recovered for over 30 min until being transferred to a recording chamber. Virus-transfected neurons were identified using IR-DIC optics and fluorescence microscopy. The recording signals were obtained using a multiclamp 700B amplifier, and sampled at 10 kHz with Digidata 1440 A. Clampfit 10.5 was used for analysis. The recording electrodes had tip resistances of 4–6 M Ω . Neurons with series resistances exceeding 20 M Ω were excluded.

For validation of the optogenetic activation, blue light (laser diode 473 nm) was delivered on the surface of the slices using a 200 mm optical fiber, and the light simulation protocols are the same as that described in the behavioral tests. For verifying the effects of the pharmacogenetic inhibition, 10 μ M CNO was perfused to the circulating ACSF after 5 min of baseline recording.

For recording spontaneous discharge rate under CHR2 stimulation⁶⁹, a blue light was delivered on the surface of brain slices using an optic fiber connected to a blue LED light (473 nm), and the light pulse (5 s duration) was controlled by the Axon pClamp software. The current-clamp recording was used to measure the action potential firing frequency of the AI or VMHvl neurons during optogenetic stimulation of the MeA OXTR neurons' terminals locating the AI and VMHvl, respectively. The recording pipette was filled with intracellular solution containing the following (mM): 130 K-Gluconate, 5 NaCl, 10 HEPES, 0.5 EGTA, 2 Mg-ATP and 0.3 Na-GTP (pH 7.3, adjusted with KOH).

For recording optically-evoked EPSC (oEPSC)⁶², 1-ms pulses of full-field illumination (10 mW mm⁻² under the objective) were delivered onto the recorded cell with a blue LED light at 30-s intervals⁶². oEPSC was recorded by holding the membrane potential of recorded neurons at –70 mV. After recording in ACSF, the slices were perfused with ACSF containing 10 μ M 6-cyano-7-nitroquinoxaline-2,3-dione (CNQX, AMPA receptor antagonist, C127, Sigma-Aldrich, USA). The same recording was performed 20 min after CNQX perfusion. The recording pipette was filled with intracellular solution containing the following (mM): 135 mM CsMeSO₃, 10 mM HEPES, 1 mM EGTA, 3.3 mM QX-314 (chloride salt), 4 mM Mg-ATP, 0.3 mM Na-GTP and 8 mM sodium phosphocreatine (pH 7.3 adjusted with CsOH).

Immunofluorescence assays

The immunofluorescence staining procedure was consistent with that previously described²⁸. Briefly, voles were anesthetized with 1.5%–3% isoflurane gas and then perfused with 50 mL 1 \times PBS (pH = 7.4–7.6) followed by 20 mL 4% paraformaldehyde (PFA) in 0.1 M PBS. After perfusion, collected brains were post-fixed overnight in 4% PFA

followed by 24 h in 15% sucrose and 24 h in 30% sucrose, then brains were embedded by Optimal cutting temperature compound (OCT, 4583, SAKURA, Japan) and cut into coronal sections by freezing microtome (CM1950, Leica, Germany). Sections were sequentially incubated in 0.3% H₂O₂ (inactivate endogenous peroxidase) and 0.3% triton X-100 for 30 min at 26 °C, and washed with 1× PBS (7 min × 3) after each step. Next, sections were blocked in 5% ready-to-use normal goat serum (AR0009, Boster Biological Technology, China) for 40 min at 26 °C and then incubated in primary antibodies overnight (anti-OXT, anti-c-Fos and anti-GABA) or for two days (anti-VGlu2 and anti-OXTR) at 4 °C. Sections were incubated in secondary antibodies with fluorescence at 26 °C for 1.5 h after washed with 1× PBS (7 min × 3). Then sections were stained by DAPI (AR1176-50, Boster Biological Technology, China) for 15 min after washed by 1× PBS (7 min × 3). Finally, sections were mounted on slides with an aqueous mounting medium (AR1109, Boster Biological Technology, China). We used a Multi-spectral tissue quantitative analysis system (OLYMPUS BX43, OLYMPUS, Japan) attached to a Nikon camera (Eclipse 80i, Nikon, Japan) to obtain images. The following image analysis was performed by image J.

The primary antibodies included: mouse anti-OXT (1:7500; MAB5296, Millipore, Germany), rabbit anti-c-Fos (1:1500, ab190289, abcam, UK), mouse anti-VGlu2 (1:500, ab79157, abcam, UK), rabbit anti-GABA (1:550, PA5-32241, Thermo Fisher, USA) and rabbit anti-OXTR (1:100, XM_041642487.1, Mabiway For Discovery, China). The production of the OXTR antibody totally followed a previous study by Professor Robert Froemke⁷⁰. Homologous OXTR amino acid sequence of voles according to epitope sequences from mice in ref. 70: KLH-CYSEGAAGGAGRAALARVS SVKLISKAKI; Contract number: MR-CY-20220604-001). The secondary antibodies (1:400): anti-rabbit goat conjugated with Cy3 (AB_2338000), AF-488 (AB_2338052), and AF-647 (AB_2338072), and anti-mouse goat conjugated with Cy3 (AB_2339065) and AF-488 (AB_2339072) were all purchased from Jackson, USA; anti-rabbit goat conjugated with AF-405 (A-48254) was purchased from ThermoFisher, USA.

Statistics

All statistical details can be found in the figure legends and supplementary Excel files of source data and statistical analysis, including the type of statistical analysis used. All data are presented as the means ± SEM. All data were assessed for normality using a one-sample Kolmogorov–Smirnov test and Levene’s test was used to confirm the homogeneity of variance. Comparisons between the two groups were performed by two-tail unpaired or paired *t*-test. One-way ANOVA or one-way repeated-measure ANOVA was used to compare multiple groups under one testing condition when appropriate. Two-way repeated-measures ANOVA was used to compare multiple groups under two testing conditions when appropriate. Post-hoc comparisons were conducted using Sidak. The significance level was set as $p < 0.05$, $^{*}p < 0.01$, $^{***}p < 0.001$, $^{****}p < 0.0001$. All of the statistical procedures were performed using SPSS (V20.0, SPSS Inc., USA). All statistical graphs/charts were plotted via GraphPad prism (V6.0, GraphPad Software, Inc., USA).

Reporting summary

Further information on research design is available in the Nature Portfolio Reporting Summary linked to this article.

Data availability

Source data are provided in this paper.

References

- Lischinsky, J. E. & Lin, D. Neural mechanisms of aggression across species. *Nat. Neurosci.* **23**, 1317–1328 (2020).
- Wu, Y. E. & Hong, W. Neural basis of prosocial behavior. *Trends Neurosci.* **45**, 749–762 (2022).
- Baron-Cohen, S. & Wheelwright, S. The empathy quotient: an investigation of adults with Asperger syndrome or high functioning autism, and normal sex differences. *J. Autism Dev. Disord.* **34**, 163–175 (2004).
- Bonfils, K. A., Lysaker, P. H., Minor, K. S. & Salyers, M. P. Affective empathy in schizophrenia: a meta-analysis. *Schizophrenia Res.* **175**, 109–117 (2016).
- Perroud, N., Baud, P., Mouthon, D., Courtet, P. & Malafosse, A. Impulsivity, aggression and suicidal behavior in unipolar and bipolar disorders. *J. Affect. Disord.* **134**, 112–118 (2011).
- Burkett, J. P. et al. Oxytocin-dependent consolation behavior in rodents. *Science* **351**, 375–378 (2016).
- Li, L. F. et al. Involvement of oxytocin and GABA in consolation behavior elicited by socially defeated individuals in mandarin voles. *Psychoneuroendocrinology* **103**, 14–24 (2019).
- Li, L. F. et al. Reduced consolation behaviors in physically stressed mandarin voles: involvement of oxytocin, dopamine D2, and serotonin 1A receptors within the anterior cingulate cortex. *Int. J. Neuropsychopharmacol.* **23**, 511–523 (2020).
- Murgatroyd, C. A. et al. Social stress during lactation, depressed maternal care, and neuropeptidergic gene expression. *Behav.-Pharmacol.* **26**, 642–653 (2015).
- Calcagnoli, F. et al. Local oxytocin expression and oxytocin receptor binding in the male rat brain is associated with aggressiveness. *Behav. Brain Res.* **261**, 315–322 (2014).
- Winslow, J. T. et al. Infant vocalization, adult aggression, and fear behavior of an oxytocin null mutant mouse. *Hormones Behav.* **37**, 145–155 (2000).
- Inoue, K., Ford, C. L., Horie, K. & Young, L. J. Oxytocin receptors are widely distributed in the prairie vole (*Microtus ochrogaster*) brain: relation to social behavior, genetic polymorphisms, and the dopamine system. *J. Comp. Neurol.* **530**, 2881–2900 (2022).
- Yoshida, M. et al. Evidence that oxytocin exerts anxiolytic effects via oxytocin receptor expressed in serotonergic neurons in mice. *J. Neurosci.* **29**, 2259–2271 (2009).
- Raam, T. & Hong, W. Organization of neural circuits underlying social behavior: a consideration of the medial amygdala. *Curr. Opin. Neurobiol.* **68**, 124–136 (2021).
- Noack, J., Murau, R. & Engelmann, M. Consequences of temporary inhibition of the medial amygdala on social recognition memory performance in mice. *Front. Neurosci.* **9**, 152 (2015).
- Gur, R., Tendler, A. & Wagner, S. Long-term social recognition memory is mediated by oxytocin-dependent synaptic plasticity in the medial amygdala. *Biol. Psychiatry* **76**, 377–386 (2014).
- Arakawa, H., Arakawa, K. & Deak, T. Oxytocin and vasopressin in the medial amygdala differentially modulate approach and avoidance behavior toward illness-related social odor. *Neuroscience* **171**, 1141–1151 (2010).
- Choleris, E. et al. Microparticle-based delivery of oxytocin receptor antisense DNA in the medial amygdala blocks social recognition in female mice. *Proc. Natl Acad. Sci. USA* **104**, 4670–4675 (2007).
- Panksepp, J. Behavior. Empathy and the laws of affect. *Science* **334**, 1358–1359 (2011).
- Nordman, J. C. et al. Potentiation of divergent medial amygdala pathways drives experience-dependent aggression escalation. *J. Neurosci.* **40**, 4858–4880 (2020).
- Wu, Y. E. et al. Neural control of affiliative touch in prosocial interaction. *Nature* **599**, 262–267 (2021).
- Gogolla, N. The insular cortex. *Curr. Biol.* **27**, R580–R586 (2017).
- Pardo-Bellver, C., Cádiz-Moretti, B., Novejarque, A., Martínez-García, F. & Lanuza, E. Differential efferent projections of the anterior, posteroventral, and posterodorsal subdivisions of the medial amygdala in mice. *Front. Neuroanat.* **6**, 33 (2012).

24. Rogers-Carter, M. M. & Christianson, J. P. An insular view of the social decision-making network. *Neurosci. Biobehav. Rev.* **103**, 119–132 (2019).
25. Kober, H. et al. Functional grouping and cortical-subcortical interactions in emotion: a meta-analysis of neuroimaging studies. *Neuroimage* **42**, 998–1031 (2008).
26. Zhang, M. M. et al. Glutamatergic synapses from the insular cortex to the basolateral amygdala encode observational pain. *Neuron* **110**, 1993–2008.e1996 (2022).
27. Falkner, A. L., Grosenick, L., Davidson, T. J., Deisseroth, K. & Lin, D. Hypothalamic control of male aggression-seeking behavior. *Nat. Neurosci.* **19**, 596–604 (2016).
28. Li, L. et al. Dorsal raphe nucleus to anterior cingulate cortex 5-HTergic neural circuit modulates consolation and sociability. *eLife* **10**, e67638 (2021).
29. Dumais, K. M., Bredewold, R., Mayer, T. E. & Veenema, A. H. Sex differences in oxytocin receptor binding in forebrain regions: correlations with social interest in brain region- and sex-specific ways. *Hormones Behav.* **64**, 693–701 (2013).
30. Nelson, R. J. & Trainor, B. C. Neural mechanisms of aggression. *Nat. Rev. Neurosci.* **8**, 536–546 (2007).
31. Chen, P. B. et al. Sexually dimorphic control of parenting behavior by the medial amygdala. *Cell* **176**, 1206–1221.e1218 (2019).
32. Cox, S. S. et al. The role of the anterior insular during targeted helping behavior in male rats. *Sci. Rep.* **12**, 3315 (2022).
33. Lin, D. et al. Functional identification of an aggression locus in the mouse hypothalamus. *Nature* **470**, 221–226 (2011).
34. Twining, R. C., Vantrease, J. E., Love, S., Padival, M. & Rosenkranz, J. A. An intra-amygdala circuit specifically regulates social fear learning. *Nat. Neurosci.* **20**, 459–469 (2017).
35. Stetzk, L. et al. Inhibiting ER α expression in the medial amygdala increases prosocial behavior in male meadow voles (*Microtus pennsylvanicus*). *Behav. Brain Res.* **351**, 42–48 (2018).
36. Maroun, M. & Wagner, S. Oxytocin and memory of emotional stimuli: some dance to remember, some dance to forget. *Biol. Psychiatry* **79**, 203–212 (2016).
37. Murakami, G., Hunter, R. G., Fontaine, C., Ribeiro, A. & Pfaff, D. Relationships among estrogen receptor, oxytocin and vasopressin gene expression and social interaction in male mice. *Eur. J. Neurosci.* **34**, 469–477 (2011).
38. Ferguson, J. N., Aldag, J. M., Insel, T. R. & Young, L. J. Oxytocin in the medial amygdala is essential for social recognition in the mouse. *J. Neurosci.* **21**, 8278–8285 (2001).
39. Samuelsen, C. L. & Meredith, M. Oxytocin antagonist disrupts male mouse medial amygdala response to chemical-communication signals. *Neuroscience* **180**, 96–104 (2011).
40. Yao, S., Bergan, J., Lanjuin, A. & Dulac, C. Oxytocin signaling in the medial amygdala is required for sex discrimination of social cues. *eLife* **6**, e31373 (2017).
41. Gu, X. et al. Anterior insular cortex is necessary for empathetic pain perception. *Brain J. Neurol.* **135**, 2726–2735 (2012).
42. Rogers-Carter, M. M. et al. Insular cortex mediates approach and avoidance responses to social affective stimuli. *Nat. Neurosci.* **21**, 404–414 (2018).
43. Craig, A. D. How do you feel-now? The anterior insula and human awareness. *Nat. Rev. Neurosci.* **10**, 59–70 (2009).
44. Molnar-Szakacs, I. & Uddin, L. Q. Anterior insula as a gatekeeper of executive control. *Neurosci. Biobehav. Rev.* **139**, 104736 (2022).
45. Méndez-Ruette, M. et al. The role of the rodent insula in anxiety. *Front. Physiol.* **10**, 330 (2019).
46. Zhang, G. W. et al. Medial preoptic area antagonistically mediates stress-induced anxiety and parental behavior. *Nat. Neurosci.* **24**, 516–528 (2021).
47. McHenry, J. A. et al. Hormonal gain control of a medial preoptic area social reward circuit. *Nat. Neurosci.* **20**, 449–458 (2017).
48. Hu, R. K. et al. An amygdala-to-hypothalamus circuit for social reward. *Nat. Neurosci.* **24**, 831–842 (2021).
49. Paletta, P., Sheppard, P. A. S., Matta, R., Ervin, K. S. J. & Choleris, E. Rapid effects of estrogens on short-term memory: possible mechanisms. *Hormones Behav.* **104**, 88–99 (2018).
50. Takayanagi, Y. et al. Activation of supraoptic oxytocin neurons by secretin facilitates social recognition. *Biol. Psychiatry* **81**, 243–251 (2017).
51. Veening, J. G. et al. Do similar neural systems subserve aggressive and sexual behaviour in male rats? Insights from c-Fos and pharmacological studies. *Eur. J. Pharm.* **526**, 226–239 (2005).
52. Delville, Y., De Vries, G. J. & Ferris, C. F. Neural connections of the anterior hypothalamus and agonistic behavior in golden hamsters. *Brain Behav. Evol.* **55**, 53–76 (2000).
53. Vochteloo, J. D. & Koolhaas, J. M. Medial amygdala lesions in male rats reduce aggressive behavior: interference with experience. *Physiol. Behav.* **41**, 99–102 (1987).
54. Luiten, P. G., Koolhaas, J. M., de Boer, S. & Koopmans, S. J. The cortico-medial amygdala in the central nervous system organization of agonistic behavior. *Brain Res.* **332**, 283–297 (1985).
55. Padilla, S. L. et al. Agouti-related peptide neural circuits mediate adaptive behaviors in the starved state. *Nat. Neurosci.* **19**, 734–741 (2016).
56. Nordman, J., Ma, X. & Li, Z. Traumatic stress induces prolonged aggression increase through synaptic potentiation in the medial amygdala circuits. *eNeuro* **7**, ENEURO.0147-20.2020 (2020).
57. Wang, L. et al. Hypothalamic control of conspecific self-defense. *Cell Rep.* **26**, 1747–1758.e1745 (2019).
58. Falkner, A. L., Dollar, P., Perona, P., Anderson, D. J. & Lin, D. Decoding ventromedial hypothalamic neural activity during male mouse aggression. *J. Neurosci.* **34**, 5971–5984 (2014).
59. Yang, C. F. et al. Sexually dimorphic neurons in the ventromedial hypothalamus govern mating in both sexes and aggression in males. *Cell* **153**, 896–909 (2013).
60. Jia, R. et al. Effects of neonatal oxytocin treatment on aggression and neural activities in mandarin voles. *Physiol. Behav.* **95**, 56–62 (2008).
61. Bian, X., Yanagawa, Y., Chen, W. R. & Luo, M. Cortical-like functional organization of the pheromone-processing circuits in the medial amygdala. *J. Neurophysiol.* **99**, 77–86 (2008).
62. Yamaguchi, T. et al. Posterior amygdala regulates sexual and aggressive behaviors in male mice. *Nat. Neurosci.* **23**, 1111–1124 (2020).
63. Miller, S. M., Marcotulli, D., Shen, A. & Zweifel, L. S. Divergent medial amygdala projections regulate approach-avoidance conflict behavior. *Nat. Neurosci.* **22**, 565–575 (2019).
64. Qian, T. et al. A genetically encoded sensor measures temporal oxytocin release from different neuronal compartments. *Nat. Biotechnol.* **41**, 944–957 (2023).
65. Li, Z. H. et al. Mesenchymal stem cells promote polarization of M2 macrophages in mice with acute-on-chronic liver failure via Mertk/JAK1/STAT6 signaling. *Stem Cells (Dayton, Ohio)* **41**, 1171–1184 (2023).
66. He, Z. et al. Paraventricular nucleus oxytocin subsystems promote active paternal behaviors in mandarin voles. *J. Neurosci.* **41**, 6699–6713 (2021).
67. Santana, N. & Artigas, F. Laminar and cellular distribution of monoamine receptors in rat medial prefrontal cortex. *Front. Neuroanat.* **11**, 87 (2017).
68. Li, L. F. et al. Reduced consolation behaviors in physically stressed mandarin voles: involvement of oxytocin, dopamine D2, and serotonin 1A receptors within the anterior cingulate cortex. *Int. J. Neuropsychoph.* **23**, 511–523 (2019).

69. Huang, T., Guan, F., Licinio, J., Wong, M. L. & Yang, Y. Activation of septal OXTr neurons induces anxiety- but not depressive-like behaviors. *Mol. Psychiatry* **26**, 7270–7279 (2021).
70. Marlin, B. J., Mitre, M., D'Amour, J. A., Chao, M. V. & Froemke, R. C. Oxytocin enables maternal behaviour by balancing cortical inhibition. *Nature* **520**, 499–504 (2015).

Acknowledgements

This research was funded by the STI2030-Major Projects grant number 2022ZD0205101 (F.T.), the National Natural Science Foundation of China grants numbers 32270510 (F.T.) and 31901082 (Z.H.), Natural Science Foundation of Shaanxi Province, China grant number 2020JQ-412 (Z.H.), China Postdoctoral Science Foundation grant number 2019M653534 (Z.H.), Fundamental Research Funds for Central University grants numbers GK201903065 (Z.H.) and GK202007008 (F.T.), and Fundamental Research Funds for Central University of China grant number GK202301012 (Z.H.).

Author contributions

F.T. and Y.Q. designed research; Y.Q. and L.Z. performed an original investigation and the majority of research; Y.Q., L.Z., W.H. performed a co-labeling experiment by AAVs (2/R); Y.Q., L.Z., L. Liu, Y. Li, L. Li, C.H., X.G., and J. Liu performed feeding voles and verification of viral efficiency; L.Z. performed in vitro electrophysiology recordings; Y.Q. analyzed data; Y.Q., L.Z., F.T., and Z.H. wrote and edited the paper. Y.Q. and L.Z. contributed equally to this work.

Competing interests

The authors declare no competing interests.

Additional information

Supplementary information The online version contains supplementary material available at <https://doi.org/10.1038/s41467-024-51652-8>.

Correspondence and requests for materials should be addressed to Zhixiong He or Fadao Tai.

Peer review information *Nature Communications* thanks Bruce Cushing, and the other, anonymous, reviewer(s) for their contribution to the peer review of this work. A peer review file is available.

Reprints and permissions information is available at <http://www.nature.com/reprints>

Publisher's note Springer Nature remains neutral with regard to jurisdictional claims in published maps and institutional affiliations.

Open Access This article is licensed under a Creative Commons Attribution-NonCommercial-NoDerivatives 4.0 International License, which permits any non-commercial use, sharing, distribution and reproduction in any medium or format, as long as you give appropriate credit to the original author(s) and the source, provide a link to the Creative Commons licence, and indicate if you modified the licensed material. You do not have permission under this licence to share adapted material derived from this article or parts of it. The images or other third party material in this article are included in the article's Creative Commons licence, unless indicated otherwise in a credit line to the material. If material is not included in the article's Creative Commons licence and your intended use is not permitted by statutory regulation or exceeds the permitted use, you will need to obtain permission directly from the copyright holder. To view a copy of this licence, visit <http://creativecommons.org/licenses/by-nc-nd/4.0/>.

© The Author(s) 2024